Near-zero-index materials for photonics

Nathaniel Kinsey[1]*, *Clayton DeVault*[2], *Alexandra Boltasseva*[3] and *Vladimir M. Shalaev*[2,3]*

Abstract | The discovery, design and development of materials are critically linked to advances in many areas of research, and optics is no exception. Recently, the spectral region in which the index of refraction of a material approaches zero has become a topic of interest owing to fascinating phenomena, such as static light, enhanced nonlinearities, light tunnelling and emission tailoring. As a result, such near-zero-index (NZI) materials bridge materials development and optical research. Here, we review recent advances in various classes of NZI platforms, with particular focus on homogeneous materials, including metals, semi-metals, doped semiconductors, phononic and interband materials, discussing the novel optical phenomena that they can produce. We also overview the developments in a key area for NZI materials, nonlinear optics, and survey some of the future goals in the field, such as the development of tailorable NZI materials in the visible range and the improvement of the theoretical description of the nonlinear enhancements in these materials.

The interaction between light and matter has long stimulated scientific discovery[1,2]. From early experiments with mirrors, lenses and prisms, researchers have learned how to engineer materials to provide a wide range of desired optical properties[3–7], even producing effects that are not achievable with natural materials[8–14]. Central to this pursuit has been the study of techniques to enhance the generally weak interaction between light and matter, allowing for a richer design space for photon manipulation and control. Among the many approaches studied is the investigation of materials in which the refractive index (n) is near zero for certain wavelengths — these materials are called near-zero-index (NZI) materials. Since the pioneering works by Nader Engheta, Richard Ziolkowski, Stefan Enoch and others[15–22], NZI materials have been shown to produce a host of fascinating and sometimes mind-bending optical effects, such as photon tunnelling[14,19,23], super-coupling[24,25], control of emission[6,15,17,26] and extreme nonlinear interactions[27–29].

The NZI condition has been realized in numerous systems, including homogenous materials (BOX 1) including metals (such as silver[30–33]), doped semiconductors (such as Al or Ga:ZnO (REFS[28,29,33,34])) and phononic materials (such as SiC (REFS[35,36])) or through structured materials (BOX 2) such as metamaterials[37–41], waveguides near the cut-off frequency[42–47], resonant cavities[48–51] and photonic crystals[16,52–56]. Although diverse, these approaches retain common features that are at the base of the unique NZI effects: diverging velocities, expansion of the wavelength and enhancement of the electric field.

Features of NZI

Diverging velocities. To illustrate the phenomenon of diverging velocities in a material with refractive index close to zero, we consider the propagation of a plane wave in a region described by a Drude oscillator (BOX 1). As $\omega \to \omega_p$ in the lossless case, where ω_p is the plasma frequency, $n(\omega) \to 0$. Thus, the phase velocity diverges ($v_p(\omega) = c/\sqrt{\varepsilon(\omega)}$ and $\varepsilon = n^2/\mu$, with c the speed of light in vacuum, ε the permittivity and μ the permeability of the material), while the group velocity:

$$v_g(\omega) = \frac{d\omega}{dk} = \frac{c\sqrt{\varepsilon(\omega)}}{\varepsilon(\omega) + \frac{\omega}{2}\frac{d\varepsilon(\omega)}{d\omega}} \quad (1)$$

tends to zero, because the slope of the permittivity is finite[57–63]. An example of diverging velocities was obtained in the optical range using a hollow metallic waveguide[42] (FIG. 1a). The silver-based structure achieved an effective NZI condition for plasmonic modes near cut-off. The waveguide was excited using a high-energy electron beam and the scattered optical emission was observed spatially and spectrally. The angular emission pattern approximates a line dipole as the wavelength approaches cut-off, demonstrating a large phase velocity for the guided mode. Furthermore, by varying the position of the electron beam within the waveguide while measuring the scattered spectral intensity, the spatial distribution of the resonant mode was observed. By combining the energy of the scattered light with the interference pattern, the momentum of the mode

[1]*Department of Electrical and Computer Engineering, Virginia Commonwealth University, Richmond, VA, USA.*

[2]*School of Physics, Purdue University, West Lafayette, IN, USA.*

[3]*School of Electrical and Computer Engineering, Purdue University, West Lafayette, IN, USA.*

**e-mail: nkinsey@vcu.edu; shalaev@purdue.edu*

https://doi.org/10.1038/s41578-019-0133-0

Box 1 | **Near-zero-index properties in homogeneous materials**

To describe the optical response and near-zero-index (NZI) properties in homogeneous materials, models such as the Lorentz model for bound electrons and vibrational (phononic) resonances and the Drude model for free electrons are used[218]:

$$\varepsilon_{r,\mathrm{Lorentz}} = 1 + \chi + \sum_i \frac{A_i}{\omega_{o,i}^2 - \omega^2 - i\Gamma_i\omega} \quad \text{(B1.1)}$$

$$\varepsilon_{r,\mathrm{Drude}} = 1 + \chi - \frac{q^2 N}{\varepsilon_o m}\frac{1}{\omega^2 + i\Gamma\omega} \quad \text{(B1.2)}$$

Here, ε_o is the free space permittivity, χ the material susceptibility at infinite frequency, A_i the strength of the ith oscillator that is governed by dipole transition rates[218], Γ the damping rate, $\omega_{o,i}$ the resonant frequency, N the free carrier density, m the effective mass of an electron $m = m^* m_o$ and q the electron charge. For each of these models (shown in the figure), there is a spectral region where the real portion of the permittivity may cross zero ($|\mathrm{Re}\{\varepsilon\}| < 1$, shaded in blue), which is called the ε-near-zero (ENZ) region[6,17,19,21] and occurs near the resonant condition for each oscillator. Although the ENZ condition is only focused on the real permittivity, very large loss values can limit its effect. As such, many works seek to minimize the loss in the ENZ regime, achieving materials with not only a vanishing permittivity but also a vanishing refractive index ($(n = \sqrt{(\varepsilon\mu)}$, shaded in red on the figure)[17,114]:

$$\mathrm{Re}\left\{\sqrt{\varepsilon}\right\} \approx \frac{1}{\sqrt{2}}\sqrt{\mathrm{Re}\{\varepsilon\} + \sqrt{\mathrm{Re}\{\varepsilon\}^2 + \mathrm{Im}\{\varepsilon\}^2}} < 1 \quad \text{(B1.3)}$$

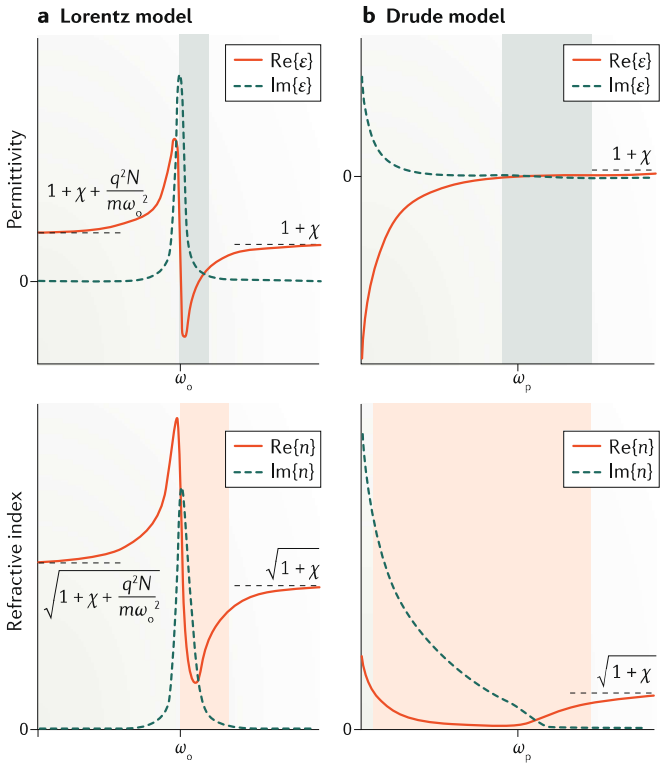

Although this condition may be realized by reducing the value of the permittivity, of the permeability (μ, to obtain μ-near-zero, MNZ, materials) or of both (to obtain ε-MNZ, EMNZ, materials[22]), the permeability of homogeneous materials in the optical range is taken as unity. The condition in Eq. B1.3 creates a range of potential combinations of the real and imaginary parts of the permittivity related by $\mathrm{Im}\{\varepsilon\} < 2\sqrt{1 - \mathrm{Re}\{\varepsilon\}}$. This condition is readily satisfied by low-loss ENZ materials. For Drude materials, it extends to real permittivity values much below zero, whereas for Lorentz materials, it is satisfied only on the blue side of the resonance frequency (shaded grey). It is important to note that, in homogeneous materials, these regions necessitate the presence of finite losses to maintain causality; thus, absorption must be carefully considered. Yet, homogeneous materials achieve ENZ and NZI properties at the local scale, as they are inherent in the material's dispersion.

NZI properties in homogeneous materials can be understood by considering the propagation of light through the material. The incident electric field polarizes the atoms, which then reradiate (scatter) the light with a frequency-dependent phase delay, $\Delta\varphi(\omega)$, determined by the loss of the oscillator γ. This process occurs many times as the light passes through the material, which effectively contributes an additional, spatially varying phase (momentum) to the propagation of the wave, $a(\omega) = (\Delta\varphi(\omega))/d$, where d is the distance between scattering events. The phase velocity becomes $v_p = \omega/(k_o - a)$, with k_o the free-space momentum; thus, it diverges when $a = k_o$, essentially the condition when the phase lag produced by the scattering events compensates for the phase gain of the wave over the same effective distance, such that the wave appears uniform over that distance. Such a large phase shift typically occurs when strong light–matter coupling is present (that is, near resonance) and dispersion results in a reduced group velocity.

was calculated to determine the waveguide dispersion ($k = m\pi/L$, where L is the length of the waveguide, in this case 2 µm). For widths smaller than 200 nm, the waveguides exhibit a cut-off mode with momentum near zero and a significantly reduced group velocity.

Additionally, a diverging phase velocity with a finite group velocity has been demonstrated by observing the refraction from a NZI metamaterial prism exhibiting a Dirac-cone dispersion[40] (FIG. 1b). Dirac-cone materials support both electric and magnetic resonances (that is, they have both $\varepsilon_{\mathrm{eff}}$ and μ_{eff}); thus, a low effective refractive index can be realized for propagating modes while maintaining a finite group velocity to facilitate transmission through the structure[40,52,64]. When the system is excited at the NZI wavelength of the prism, the phase velocity diverges, producing a wave with nearly uniform phase across the prism. As a result, the wavefront (and refraction angle) is defined by the shape of the flat exit facet, which produces a large anomalous refraction at 0°.

Diverging velocities are a central feature of NZI materials, because they result in a strong enhancement of light–matter interactions[65,66]. Consequently, they have been explored across a wide range of optical applications, including sensors[60], cloaking and transformation optical devices[45,46], near-perfect optical absorbers[67], optical memories[68–71], systems with enhanced quantum interactions[40,72,73] and nonlinear interactions[28,29,74–78], as well as pulse shaping[74,79].

Wavelength expansion. Substantial wavelength expansion in NZI materials is a natural consequence of the diverging phase velocity. $\lambda_{\mathrm{NZI}} = \lambda_o/n$ (λ_{NZI} is the wavelength at which n approaches 0 and λ_o the free-space wavelength); thus, when the refractive index n is small, the wavelength increases drastically. The consequence is a surprisingly small — almost negligible — phase advance ($kL = 2\pi L/\lambda_{\mathrm{NZI}} \to 0$) of the wave propagating through a NZI film with thickness L much larger than the free-space wavelength. The phenomenon of

Box 2 | **Near-zero-index properties in structured materials**

In structured materials, the near-zero-index (NZI) condition is achieved through the careful design of the microstructure or nanostructure of the material, as the constituent materials generally do not exhibit NZI effects within the region of interest. One approach is effective medium theory, a technique exploited in many optical metamaterials. Here, the permittivity of a system of two intermixed materials is given by $f\frac{\varepsilon_1-\varepsilon_{eff}}{\varepsilon_1+2\varepsilon_{eff}}+(1-f)\frac{\varepsilon_2-\varepsilon_{eff}}{\varepsilon_2+2\varepsilon_{eff}}=0$, where f is the volumetric filling fraction[269], ε_1 and ε_2 are the permittivities of the two constituent materials and ε_{eff} is the effective permittivity of the metamaterial; all permittivities may be complex. By properly mixing a material with a negative permittivity and one with a positive permittivity (for example, alternating layers of a metal and a dielectric), an effective NZI or ε-near-zero (ENZ) region can be obtained. Although somewhat challenging in the optical range owing to the large magnitude of metallic permittivity, this approach has been investigated in systems including nanoparticle composites, rod structures and lamellar layers[37,38,269–271].

Another approach is to manipulate the geometry of a guiding structure. As an example, we consider the dispersion of a transverse magnetic mode, TM_{10}, in a metallic rectangular waveguide in which $k=k_o\sqrt{(1-(\lambda/2a)^2)}=k_o n_{eff}$ (REF.[90]), with k_o the free-space momentum and n_{eff} the effective refractive index. When the height of the waveguide a approaches half of the wavelength λ, the momentum k tends to zero, producing an effective mode index of zero (panel **a** of the figure, orange and red curves to the left of the light line).

Another interesting condition can be found in thin films characterized by a Drude dispersion[43,272]. For very thick films ($d\to\infty$), the dispersion approximates a semi-infinite surface plasmon dispersion (red solid line). As the film's thickness is decreased past the skin depth, the surface plasmons at each interface begin to interact and form two branches, the long-range and short-range surface plasmon polaritons, whose dispersion varies with thickness (dashed orange curves for 150-nm films). For ultrathin films, such as the $d=2$-nm film corresponding to the green curve, the long-range mode becomes nearly flat and asymptotically approaches the dispersion of the plasma frequency within a range of wave numbers. This mode occurs at exactly the frequency at which the permittivity is approximately zero and is referred to as the ENZ mode. Above the plasma frequency, the bulk plasmon branch also exhibits a flat dispersion near the plasma frequency and is denoted as either the Berreman or the Brewster mode[43,109,272–274]. These modes exhibit directional-dependent perfect absorption at frequencies corresponding to $\mathrm{Im}\{\omega\}=0$ (REFS[67,275]). Similar conditions can be found for modes in dielectrics cladded with NZI materials, in fibre-based platforms[276] or in broadband super-octave absorbers through an asymmetric Fabry–Pérot cavity metasurface[277].

Yet another approach is the use of resonant structures, such as a stack of dielectric resonators (panel **b** of the figure). When the size of the resonators becomes comparable to the wavelength, the optical response is described by Mie theory[278]. Excitations produce electric resonances due to the linear polarization of the dielectric by the electric field, and magnetic resonances due to the formation of whispering gallery modes[50,64,230,279–281]. These resonances result in a reradiation of the field (scattering) with some finite phase shift, and multiple scattering events produce a growing phase delay. If the size of the resonators a is much smaller than the wavelength ($k_o a\leq 1$), we may define an effective permittivity and permeability (generally following a Lorentzian dispersion) related to the phase shift expected over the thickness of the effective medium, $\Delta\varphi=n_{eff}k_o t$. By properly controlling the structure of the resonators, the refractive index, permittivity and permeability can be simultaneously (NZI, ε-μ-near-zero materials) or independently (NZI, ENZ, μ-near-zero materials) brought close to zero while maintaining control over the impedance $Z=\sqrt{(\mu_{eff}/\varepsilon_{eff})}$. Similar conditions can be realized in plasmonic metamaterial structures[269,282,283] and in so-called Dirac-cone 2D photonic crystals[40,55,64].

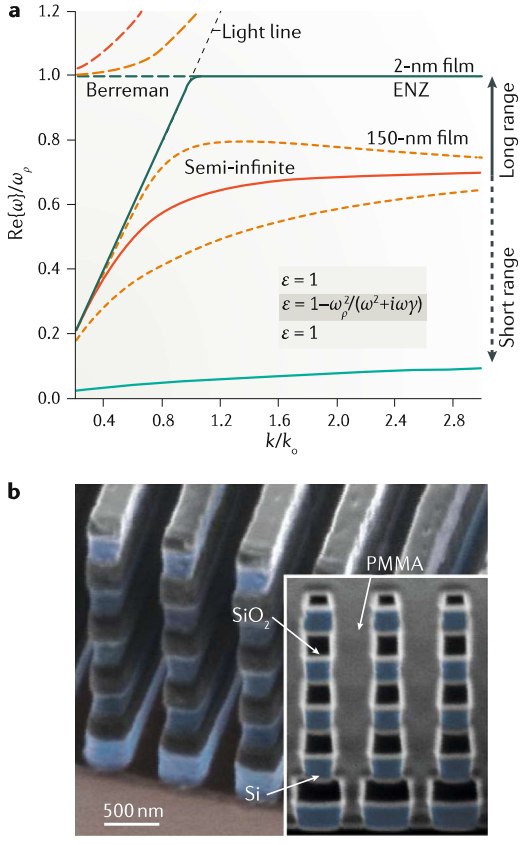

Panel **b** is adapted from REF.[64], Springer Nature Limited.

wavelength expansion in NZI materials was observed using a corrugated waveguide structure that achieved the NZI condition through a Dirac-cone optical dispersion[55] (FIG. 1c). When the excitation wavelength at both ends of the waveguide was tuned towards the point of zero-mode index (excitation wavelength of 1,625 nm), an interference pattern with diverging beat length was observed, indicating negligible phase advance over large distances. Interestingly, this phenomenon is readily observed using standard objectives, because the expansion of the wavelength results in standing waves with nodes that are larger than the diffraction limit in free space. This diverging wavelength effect has been used to achieve phase-matching-free nonlinear optical devices[23,27,80–83], super-coupling[19,20,41,84,85], antenna resonance pinning[26,86,87] and geometry-invariant cavities[88].

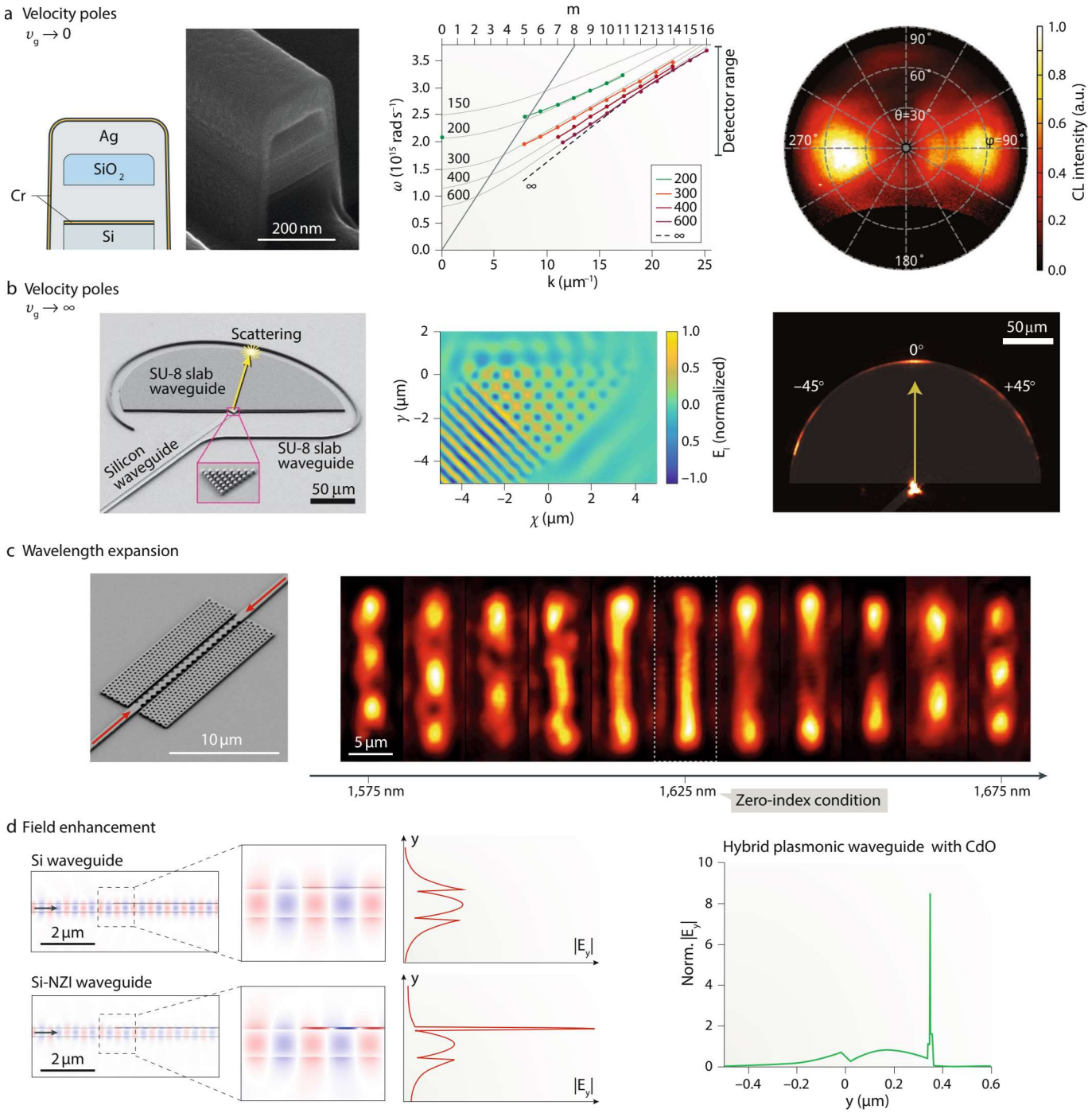

Fig. 1 | **Overview of the effects observed in near-zero-index materials.** **a** | Scanning electron microscope image of a silver plasmonic waveguide that guides confined plasmonic modes within the SiO_2 gap. As the excitation approaches the cut-off frequency of the waveguide (dispersion plot, centre), the group velocity and effective mode index tend to zero, producing a nearly uniform phase across the structure and a directional radiation pattern equivalent to a line dipole (right). **b** | Scanning electron microscope image (left) of an on-chip, zero-index metamaterial prism placed at the end of a silicon waveguide with an SU-8 slab guiding region and a circular scattering element. When excited through the silicon waveguide from the bottom left, the light enters the prism and refracts at an angle determined by momentum matching. As the excitation wavelength approaches the zero-index region, the phase velocity tends to infinity and a nearly uniform phase is achieved within the prism, as shown by the simulated interference pattern (centre), which results in emission leaving in the direction normal to the interface instead of at an arbitrary angle (right). **c** | The wavelength tends towards infinity in a metamaterial waveguide with counterpropagating modes. The beat length of the interference pattern (described by the wavelength of the mode) extends greatly as the excitation wavelength approaches the zero-index condition. **d** | Field enhancement of the normal component of the electric field in near-zero-index (NZI) materials. For a wave propagating in a silicon waveguide, when a NZI layer is placed on top of the waveguide, a strong field confinement is observed. Wrapping a layer of CdO around the waveguide also results in strong confinement of the normal component of the electric field and gives rise to compact and efficient optical amplitude and phase modulation devices. CL, cathodoluminescence. Panel **a** is adapted with permission from REF.[42], copyrighted by the American Physical Society. Panel **b** is reproduced from REF.[40], Springer Nature Limited. Panel **c** is reproduced with permission from REF.[55], ACS. Panel **d** is reprinted with permission from REF.[91], OSA.

It was also the focus of interesting theoretical work on 'DC' or 'static' light[89].

Field enhancement. Finally, an electric field (E) enhancement occurs in the material due to the electromagnetic boundary conditions[90], requiring that the normal component of the electric field across a boundary in a charge-free region in an isotropic material obeys the relationship $\varepsilon_1 E_1^{\perp} = \varepsilon_2 E_2^{\perp}$. This results in the enhancement of the normal component of E inside the NZI material, $E_2^{\perp}$, by a factor of $\varepsilon_1/\varepsilon_2$. Because $\varepsilon_2 \to 0$, an effective confinement of energy inside the NZI layer is realized. This effect is illustrated for a propagating photonic mode in a silicon waveguide cladded with air (FIG. 1d). When a small layer of NZI material is placed on top of the waveguide, a sharp region of high electric field is observed, in which light is confined. This effect was utilized by combining a high-mobility (250 $cm^2 V^{-1} s^{-1}$), dynamically tunable cadmium oxide layer with a hybrid plasmonic waveguide[91–94]. When an electric field was applied across the CdO layer, electrons accumulated within the material and formed a thin NZI region, which, owing to the boundary conditions associated with NZI materials, caused a large portion of the light to be confined within the dynamic CdO layer. Unlike in previous experiments, in which similar devices were used to produce amplitude modulation, high-mobility CdO can achieve a low-loss operational condition such that efficient phase modulation is possible. A modulation efficiency $V_\pi L_\pi$ of 0.005 V cm was predicted, compared with 1.8 V cm in lithium niobite modulators[95]. This confinement effect has been central to the enhancement of light–matter interactions, enabling extreme, nonlinear optics[29,61,74,96–98] and integrated nanophotonic devices[99–103], in which a key feature is the ability to dynamically control the NZI or ε-near-zero (ENZ, BOX 1) condition by electrical or optical means[28,74,104,105].

Realizing near-zero-index materials

There are many approaches to realizing NZI properties, each with their own trade-offs. Structured materials (metamaterials, composites and waveguides) provide advantages such as extreme tunability in the near-zero condition and a bandwidth that can be engineered by controlling the geometry and constituent materials. Furthermore, the ability to control both the permeability and permittivity of some structures allows for a diverging phase velocity with a finite group velocity and impedance, resulting in NZI, ENZ, μ-near-zero (MNZ) and ε-MNZ (EMNZ) materials[22,40,55,64]. This is important for applications in which efficient transmission through the NZI layer is desired, such as waveguiding, nonlinear frequency conversion and optical pulse shaping. Yet, these benefits are achieved at the cost of significantly increased fabrication costs and complexity.

NZI effects can also be mimicked in other structured materials, in which they have a fundamentally different origin. For example, random photonic structures can produce strong light–matter interactions[106–108]: the multiple scattering events can be viewed as an effective reduction in the group velocity of the light passing through the material. Similarly, photonic crystals can exhibit extreme slow-light phenomena[56,70]. As the frequency of light approaches the band edge of the material, the dispersion of modes within the crystal flattens (due to the coupling of forward-propagating and backward-propagating modes), reducing the group velocity by a factor of over 100 while maintaining a finite momentum[56].

However, structured materials can achieve NZI behaviour only as an effective property, occurring on distances larger than the size of the structural unit. Conversely, homogeneous (non-structured), naturally occurring NZI materials achieve this property locally, which is beneficial for combining NZI phenomena with nanoresonators and quantum emitters. Furthermore, they can be realized in a simple thin film with relatively low losses, which can be readily combined with other structures, such as metasurfaces[26,109,110] and guiding structures[101,103,111,112]. However, a key limitation of homogeneous materials is the impedance mismatch incurred when realizing low-loss NZI materials, as the impedance tends towards zero or infinity ($Z = \sqrt{(\mu/\varepsilon)}$).

From this perspective, NZI materials can be viewed as a subset of a more general class of materials that realize light–matter enhancement through slow light, and the optimal approach depends on the application and desired outcome[61–63,65,66,113]. Here, we focus on the development of homogeneous NZI materials, discussing the advantages of Drude-based and resonant-based approaches to achieve a NZI or ENZ response. We also overview the optical losses at the crossover wavelength (the wavelength at which the real part of the permittivity changes sign) and discuss associated trends. More information on the advances in structured NZI and ENZ materials and in MNZ and EMNZ materials can be found in other reviews[98,114].

Metals. Metals exhibit a large free-carrier density ($5–10 \times 10^{22}$ cm^{-3}) and their optical properties are largely dominated by Drude dispersion. As a result, ENZ properties occur naturally, with many materials exhibiting a crossover from positive to negative values of the real part of the permittivity in the visible and ultraviolet spectral range[115–120] (FIG. 2, circles). However, in many metals (for example, titanium, thallium, tungsten and zinc), the crossover wavelength is located in the deep ultraviolet due to the large intrinsic carrier density. Although such metals can achieve the ENZ condition, and some can reach the NZI condition, they have not been explored in detail owing to the short wavelengths required. Gold and silver are an exception, with an ENZ region at 520 nm for gold (with ε_{co}'', the value of the imaginary permittivity at the crossover wavelength of the real permittivity, equal to 3) and at 362 nm for silver ($\varepsilon_{co}'' = 0.5$), wavelengths readily accessible in optical experiments.

Nonlinear optical processes in gold in the ENZ regime have been studied for many years[121]. Preliminary works were motivated by the exploration of the nonlinearity in the vicinity of the interband transition, but an NZI and ENZ region arises in the same spectral window. The nonlinear interaction in gold films was observed using Z-scan at 532 nm; the refractive index was found to be $\tilde{n} = 0.5 + 2.0i$ and the third-order susceptibility $\tilde{\chi}^{(3)} \approx (-3.4 + 0.8i) \times 10^{-15}$ $m^2 V^{-2}$, 6–7 orders of magnitude

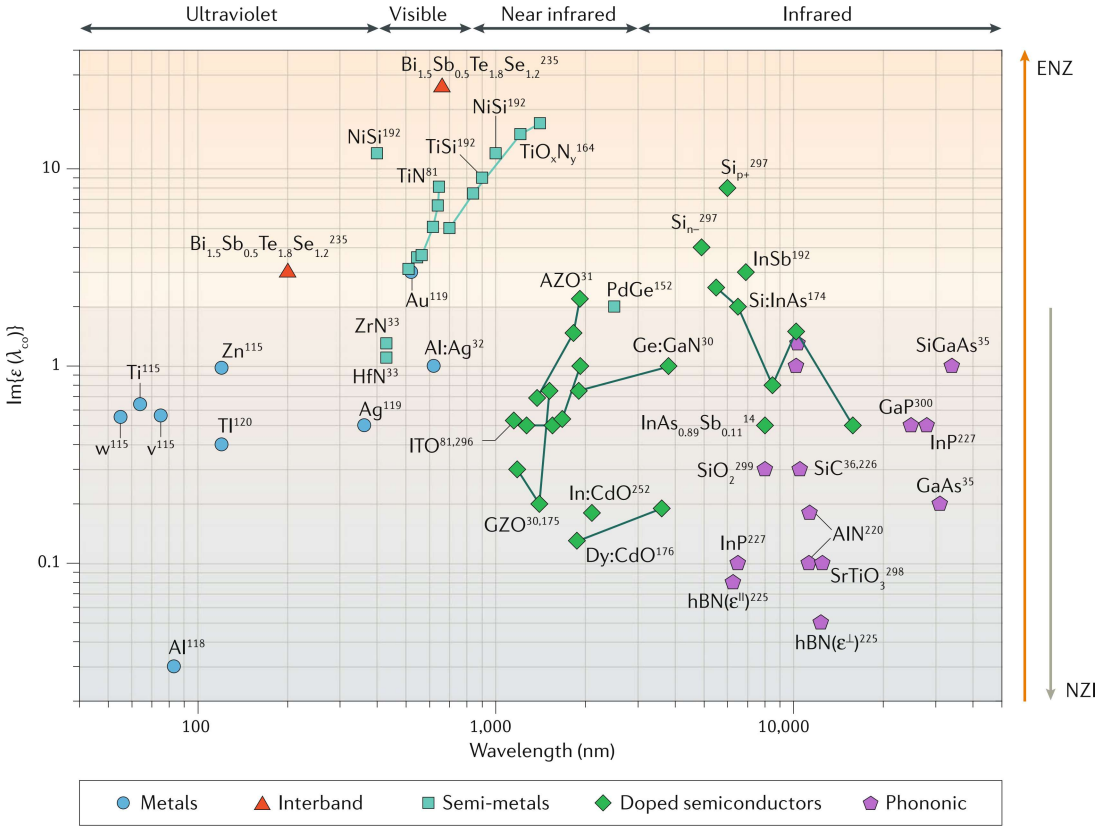

Fig. 2 | **Comparison of experimentally realized bulk homogeneous ε-near-zero and near-zero-index materials.** The value of the imaginary permittivity ε is plotted at the crossover wavelength (λ_{co}) at which the real permittivity is zero. Materials with an imaginary permittivity smaller than 2 at the crossover wavelength exhibit near-zero-index (NZI) properties. The lines connect the different measured values of Im{ε} for a given statically tunable material and illustrate their variability. ENZ, ε-near-zero; hBN, hexagonal boron nitride.

larger than that of silica[122]. Furthermore, theoretical calculations show that this large enhancement coincides with the NZI region in the film[123]. Nonlinear studies on gold films are summarized in REF.[124]. Moreover, the expansion of the wavelength combined with the tight confinement in the ENZ range has motivated theoretical studies of non-local effects in metals and of their potential role in applications such as superlensing, waveguiding and quantum plasmonics[125–127].

An alternative approach would be to forgo NZI effects (slow light and wavelength expansion) and focus on the confinement and impedance effects achieved in the ENZ region. A material realizing these properties, presumably with large optical losses, would be quite efficient as an absorber and useful for applications such as hot-electron generation[128], photocatalysis[129], local heating and nanoparticle trapping[130–132]. In this sense, chromium may be an interesting metal for broadband ENZ-enhanced absorption, because it possesses a weakly negative and relatively flat permittivity across the visible and near-infrared spectrum[117].

Despite their potential applications and interesting physics, ENZ and NZI effects in metals are largely under-investigated. Research has instead focused on utilizing them as constituent materials for metamaterials and structured ENZ approaches, and on exploring their plasmonic properties for other nanophotonic applications[92]. However, the development of 2D materials has led to the exploration of ultrathin[133] and 2D metallic films, such as stanene (2D α-tin(111))[134–136], borophene (2D boron)[137] and argentene (2D silver)[138], and of their optical properties. Theoretical predictions suggest significantly reduced optical loss factors in these 2D metals as compared with their bulk counterparts, in addition to new and interesting physics that can be combined with NZI and ENZ properties to explore extreme confinement of light and the enhancement of light–matter interactions[134,136,138,139]. Furthermore, theoretical predictions show that a bulk lossless metal can be achieved within a given frequency band by manipulating the relative energy-band offsets[140]. However, it is important to note that a key limitation of metals is the lack of spectral tunability of the ENZ condition. Although alloying and annealing of films have been used to demonstrate tunability of noble metals such as silver (the crossover wavelength, λ_{co}, varied from 350 nm to 600 nm)[32,141] and gold (λ_{co} varied from 440 nm to 500 nm)[142,143], this tunability is, in general, limited in range and produces loss factors comparable to or larger than those of the pure metals. Another approach is to realize ultrathin, trans-dimensional films with a thickness of only a few atomic layers and properties in between those of 2D and 3D materials[144]. In such thin films, the optical properties can be tuned by applying electrical, optical and mechanical

stress or strain. This added tunability may provide a unique opportunity to vary the NZI and ENZ region in these materials.

Semi-metals. By combining elemental metals with semiconducting and dielectric elements, semi-metals are obtained, with a carrier density that is reduced ($1–5 \times 10^{22}$ cm^{-3}) compared with that of a pure metal, facilitating permittivity crossovers within the visible spectrum[30] (FIG. 2, squares). A recent focus on the development of such semi-metals has identified vast families of materials (such as silicides[145–147], transition-metal nitrides[31,33,148–151], germanides[152,153] and hydrides[154]) that exhibit metallic properties across the ultraviolet–near-infrared spectrum.

Among these materials, transition-metal nitrides have demonstrated promise for nanophotonic applications in the visible range and have been widely studied[148,155–159]. They comprise various metallic compounds, such as TiN ($\lambda_{co} = 500$ nm, $\varepsilon_{co}'' = 3$), ZrN ($\lambda_{co} = 430$ nm, $\varepsilon_{co}'' = 1.1$) and HfN ($\lambda_{co} = 430$ nm, $\varepsilon_{co}'' = 1.3$), and provide the opportunity to explore ENZ effects within the blue–green region. Several other compounds, such as VN, YN and WN, are predicted to exhibit similar properties[160] but have yet to be rigorously studied experimentally. The loss factors of the explored transition-metal nitrides are presently too large to enable deep NZI effects, although ZrN and HfN achieve a weak NZI condition in the visible range with theoretical predictions demonstrating the potential for improvement[160].

A recent intersection between semi-metals and ENZ behaviour lies in the theoretical investigation of on-chip quantum networks in TiN (REFS[161,162]). The supercoupling effect[20] that occurs in the NZI and/or ENZ region, in which waves can propagate through subwavelength features and around sharp bends without reflection, is exploited to significantly shrink the footprint of the overall network and provide near-synchronous excitation of multiple quantum emitters. Although the loss in the TiN sample studied is large ($\varepsilon_{co}'' = 4$), the coherence length of the mode (~400 nm) is roughly 40 times larger than in noble metals, making TiN an interesting material for visible-spectrum quantum networks, in which numerous room-temperature quantum emitters, such as nitrogen-vacancy centres, operate[163]. In the same work, a simulation of a 5×5 grid occupying a 15×15-μm^2 area and containing 25 quantum emitters revealed that the electric field is well distributed with nearly uniform phase, enabling coherence across the network. However, it is clear that losses will be a challenge in this system, and the structures and materials should be optimized.

Beyond extending ENZ properties across the visible and near-infrared ranges, an advantage of semi-metals is that their stoichiometry and structure can be manipulated to broadly tune the crossover point; dynamic tuning through electrical and optical excitations is also possible. Control over the deposition ($\Delta\lambda_{co} = 710$ nm)[164] and annealing conditions ($\Delta\lambda_{co} = 2{,}200$ nm)[152] and the introduction of ternary compounds ($\Delta\lambda_{co} = 140$ nm)[165] have been exploited to this end. This tunability allows the design of these materials for specific applications. This was demonstrated, for example, by controlling the deposition of metal ceramics: by mixing TiO_2 and TiN, a double-crossing ENZ material was obtained[164]. It was suggested that the double-crossing behaviour is a result of small TiN inclusions in a TiO_2/TiO_xN_y host that provides plasmonic resonances. The control over nitrogen pressure allowed for substantial tuning of the ENZ region, producing an extremely wide and tunable ENZ bandwidth (650–1,400 nm), although the region has large optical losses. Such a broad ENZ region and the corresponding enhanced absorption may be useful for improved materials for water splitting, an application in which TiN and TiO_2 structures have shown promise[166–168]. More information on the development of semi-metals for optics can be found in REF.[30].

Doped semiconductors. Arguably the most versatile and widely studied NZI and ENZ materials are doped semiconductors. In particular, doped oxides[33,34,169–171], nitrides[172,173] and arsenides[14,174] are studied for their NZI properties (FIG. 2, diamonds). Doped semiconductors exhibit several attractive properties: broad tunability of the NZI and ENZ condition; low losses at the crossover point; wide NZI and ENZ region bandwidth due to Drude response; and static and dynamic tunability of the NZI and/or ENZ region. Moreover, they comprise a wide range of material classes and can be fabricated using well-developed protocols, both as single crystals and epitaxial materials. Highly doped oxides (such as In:SnO, Ga:ZnO and In:CdO) can reach a permittivity crossover up to the edge of the visible spectrum (~1,150 nm)[81], whereas Si:InAs reaches a permittivity crossover into the far-infrared (15,800 nm)[174]. By varying the base material, composition and doping level, the entire spectral range between these values can be covered.

In the near-infrared spectral range, highly doped oxides such as In:SnO, Al:ZnO and In:CdO have been heavily studied, largely owing to their low optical losses (Ga:ZnO: $\lambda_{co} = 1{,}180$ nm, $\varepsilon_{co}'' = 0.3$ (REFS[74,175]); Dy:CdO: $\lambda_{co} = 1{,}870$ nm, $\varepsilon_{co}'' = 0.13$ (REF.[176])) and a NZI and/or ENZ range that coincides with the telecommunication spectrum (for example, Al:ZnO has $\lambda_{co} = 1{,}300$ nm and $\varepsilon_{co}'' = 0.3$ (REF.[28])). The presence of NZI and ENZ properties in this technologically important spectral range, combined with enhanced nonlinearities, has led to significant efforts to develop communications devices controlled electrically and optically[26,28,29,74,104,105,177,178]. A thin layer of In:SnO sandwiched between a silicon rib waveguide and a gold cap was recently used to demonstrate a compact, on-chip, hybrid plasmonic optical switch[179] (FIG. 3a). The confinement of the light in the plasmonic section allows strong modulation to occur within a small footprint, reducing the energy consumption and increasing the speed of the device. Under a 2-V electrical bias between the silicon and the gold, the In:SnO accumulates electrons and the refractive index of a small region of the device is biased into a NZI condition. As a result, light becomes strongly confined within the NZI region of the indium tin oxide (ITO), where it is absorbed (6.5-dB extinction ratio in 4 μm at a speed of 2.5 GHz). Modulator designs using NZI and ENZ materials have been previously proposed and demonstrated at low

speed. However, ion and trap state migration[104,180] have led to difficulties in demonstrating reliable and impactful performance at high speeds, which was overcome in this work. More information on active devices for telecommunication based on NZI materials can be found in the reviews in REFS[92,103,181].

These oxides host other interesting phenomena. Gold antennas with lengths varying from 300 nm to 800 nm were fabricated on Al:ZnO and Ga:ZnO substrates[26]. When the scattering spectrum of the antennas was measured, it was observed that they all exhibited a resonance that coincided with the permittivity crossover of the substrate (FIG. 3b). This occurs because, at the NZI point, the wavelength diverges, producing a strong electric dipole resonance within the nanoantenna, independent of its size. The length-independent character of the dipole resonance was subsequently confirmed using scanning near-field optical microscopy to determine the

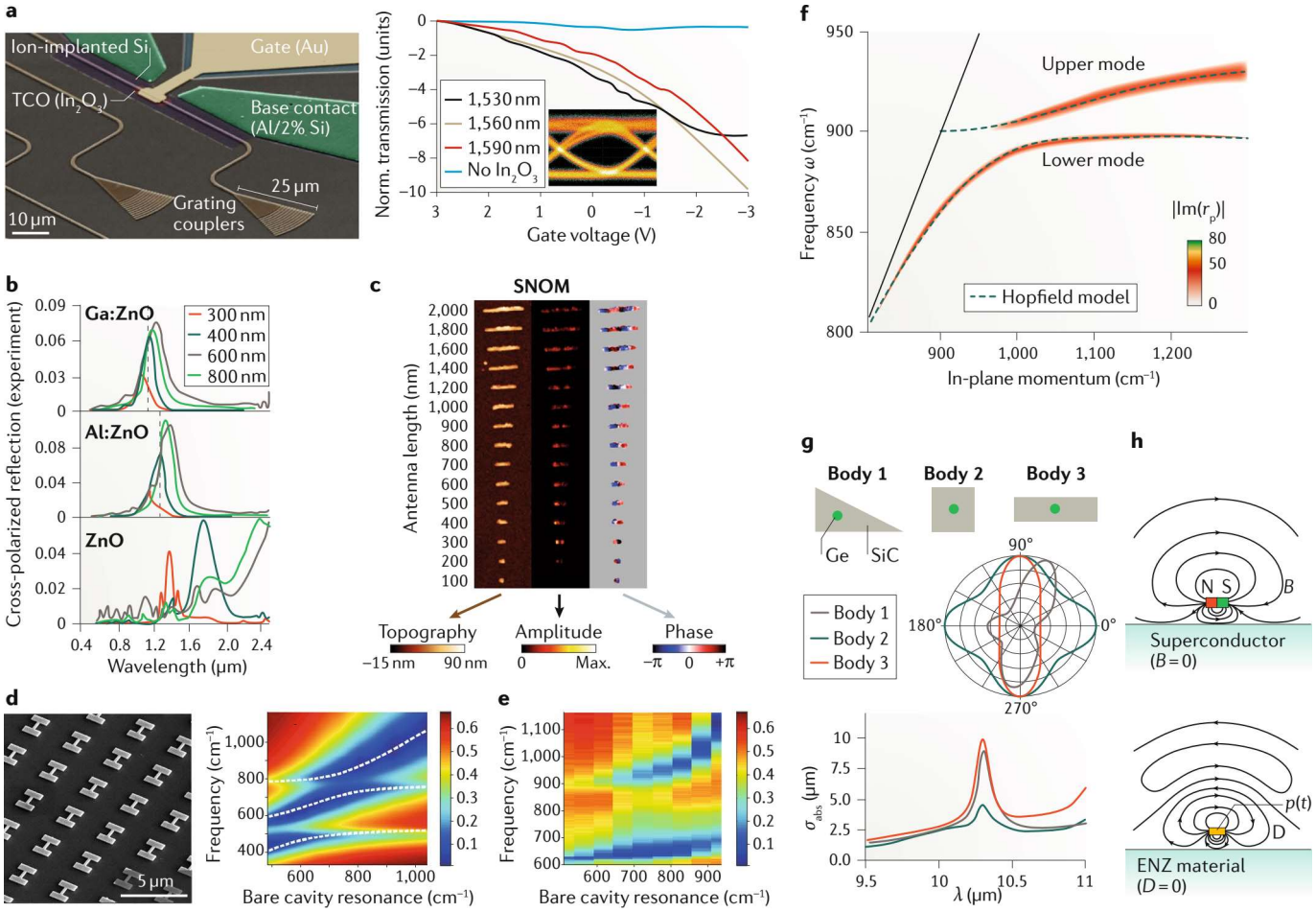

Fig. 3 | **Studies of near-zero-index and ε-near-zero properties in homogeneous materials. a** | False-colour scanning electron microscope image of a nanophotonic modulator utilizing a dynamic near-zero-index (NZI) layer (left). The device achieves large modulation (−10 dB) at the NZI wavelength of 1,560 nm, as shown by the transmission reduction versus applied DC voltage (right), and is suitable for high-speed (>2 GHz) operation, as shown by the eye diagram inset. **b** | Reflection spectra from plasmonic antennas on NZI substrates (Al:ZnO and Ga:ZnO) and on a reference substrate (ZnO). The resonance of all antennas is pinned to the NZI region, independent of their size. **c** | Scanning near-field optical microscopy (SNOM) images showing the dipolar resonance of the plasmonic antennas on an Al:ZnO NZI substrate, showing that the resonance does not depend on the size of the antennas. **d** | A scanning electron microscope image (left) of a resonant plasmonic metasurface fabricated on a quantum well structure, with a doped InGaAs ε-near-zero (ENZ) layer in between. The metasurface and ENZ region are detuned from the quantum well structure and produce two strong-coupling regions, as observed in the simulated transmission maps (right). **e** | The transmission spectrum of the same metasurface/ENZ/quantum well structure measured when the ENZ layer is brought in-resonance with the quantum well transitions shows the suppression of the middle absorption branch. **f** | Strong coupling between a silicon carbide surface phonon polariton and the ENZ mode of an ultrathin film of aluminium nitride. The strongly coupled system exhibits a large splitting at the degenerate ENZ frequency, which is modelled accurately using the Hopfield model for two oscillators. r_p is the p-polarized reflection coefficient. **g** | Illustration of silicon carbide cavities with different cross sections with an embedded germanium rod. The cavities improve, shape and provide enhanced coherence to random thermal emitters placed within them, as seen from the emission pattern at the ENZ wavelength and from the absorption cross-section σ_{abs} for thermal emission. **h** | Illustration of electric levitation using ENZ materials; a field profile similar to that used for magnetic levitation is obtained, which results in a repulsive force between the ENZ substrate and a dipole emitter. Panel **a** is reprinted with permission from REF.[179], OSA. Panel **b** is reprinted with permission from REF.[26], OSA. Panel **c** is reprinted with permission from REF.[182], OSA Panels **d** and **e** are adapted with permission from REF.[44], copyrighted by the American Physical Society. Panel **f** is reproduced with permission from REF.[228], ACS. Panel **g** is reproduced with permission from REF.[229], PNAS. Panel **h** is adapted with permission from REF.[232], copyrighted by the American Physical Society.

spatial phase of the resonance[182] (FIG. 3c). At the NZI wavelength, a strong reduction in the near-field coupling of dimer antennas was also observed, which is advantageous for improving fabrication tolerance, device robustness and developing dynamic sensors. The use of doped semiconductors such as In:SnO has also been explored for tuning both dielectric and plasmonic metamaterials[105,183]. NZI materials provide efficient tuning of dielectric metamaterials made from silicon (31% modulation depth) by facilitating the extraction of the energy of the resonant mode from the dielectric antenna[184]. For plasmonic metasurfaces, the large change in local refractive index under dual-gate electrical bias provides a strong shift in the antenna resonance, enabling a tunable phase shift greater than 300° and a reflectance modulation of 90%[185]. More information on the use of NZI materials for metamaterial tuning can be found in the reviews in REFS[13,186].

Another interesting phenomenon in doped semiconductors is the excitation of ENZ and Berreman modes[24,43,44,67,83,109,187]. A key feature of these modes is the near-perfect and spectrally sharp absorption obtained in deeply subwavelength NZI films[188]. This is accomplished by coupling to plasma oscillations with wave vectors above (ENZ modes) or below (Berreman modes) the substrate and superstrate light lines, which exhibit low group velocity at the permittivity crossover (BOX 2). These modes exhibit strong polarization-dependent and directional-dependent absorption that may prove useful for various filtering applications. Perfect absorption coincides with the transition from bound to leaky modes, happening when $\mathrm{Im}\{\omega\} = 0$ (REF.[67]) (BOX 2). The application of ENZ and Berreman modes for perfect light absorption was demonstrated in an ultrathin In:SnO film that could be tuned via doping concentration and electrical bias; a shift of 20% of the perfect absorption wavelength was obtained[189]. Although this effect has been first demonstrated in doped oxides, the results are general and perfect absorption is achievable in many materials that exhibit a NZI point.

Low-doped semiconductors such as ZnO (REF.[190]), InAs (REF.[174]) and Si (REF.[191]) can achieve crossover points in the mid-infrared spectral range[192]. This is useful for bringing ENZ and NZI properties to an entirely new set of applications related to thermal imaging, chemical sensing and vibrational spectroscopy. Additionally, due to the reduced carrier density, the Drude losses are, in general, smaller as compared to those in highly doped semiconductors. NZI effects were obtained in semiconductors with loss factors below unity[175,193].

The complex coupling of metamaterial, intersubband and ENZ modes in doped semiconductors has been studied in a plasmonic metasurface fabricated on a quantum well structure[44]. In this type of system, strong coupling between the resonant modes of the metastructure and the quantum wells can produce unwanted Rabi splitting. The transmittance of the structure can be tailored by adding a layer of doped InGaAs between the metasurface and the quantum wells. Initially, three strongly interacting dispersion branches are observed (FIG. 3d). The first shows an anti-crossing point near 600 cm^{-1}, which arises due to the coupling of the ENZ mode with the metamaterial resonators, whereas the second crossing occurs near 800 cm^{-1} and is due to intersubband transitions in the quantum wells. However, when the doping of the InGaAs ENZ layer is adjusted to coincide with the intersubband transitions at 800 cm^{-1}, the central dispersive branch disappears and the splitting between the metamaterial and intersubband transitions widens (FIG. 3e). In this case, by tuning the permittivity of the InGaAs layer either electrically or optically, the coupling of the various resonators can be adjusted and the transmittance greatly modified. Furthermore, the ENZ layer serves to relay and enhance the out-of-plane component of the electric field produced by the metasurface due to the boundary conditions. This results in a stronger interaction between the two resonances, whose tunability may be useful for enhanced nonlinear effects[133], spectral filters[194] or tailored light emission[195].

Building on decades of academic and industrial development of semiconductors, a wide range of material platforms are available, fabricated with many established methods, including sputtering[31], laser ablation[196], chemical vapour deposition[197], molecular beam epitaxy[34] and liquid chemistry[170], which can produce both polycrystalline and single-crystalline films, as well as nanoparticles[170] and nanorods[171,177]. In particular, In:SnO and ZnO blends have been well studied owing to their use as transparent contacts for displays, touchscreens and solar cells, as well as in high-quality blue LEDs[198–204]. These efforts have produced well-understood growth methodologies[33,169,175,205–207], enabling, for example, the formation of monolithic, single-crystal, low-defect ZnO on c-plane and a-plane sapphire with highly doped Ga:ZnO contacts with appreciable mobility (45 $\mathrm{cm}^2\mathrm{V}^{-1}\,\mathrm{s}^{-1}$)[198,208,209]. By contrast, in other works, ZnO, Al:ZnO and Ga:ZnO are deposited using pulsed-laser ablation of a blended target under extreme oxygen deprivation, producing materials with significant defect concentrations[33]. This morphology variation is a key feature for interband nonlinear processes (BOX 3), in which defects facilitate enhanced recombination rates for sub-picosecond switching[28]. Similar growth-optimization procedures can be completed for other materials classes, focusing on key areas such as reducing losses and improving tunability and substrate compatibility, although specific goals may vary based on the intended application.

In:SnO has shown the shortest crossover wavelengths, approaching 1,100 nm (REFS[30,81]), whereas CdO blends, including Dy:CdO, In:CdO and Y:CdO, which have exceptionally high mobilities ($\mu = 250$–$500\ \mathrm{cm}^2\,\mathrm{V}^{-1}\,\mathrm{s}^{-1}$ (REFS[176,210,211]) compared with $\mu = \sim 45\ \mathrm{cm}^2\,\mathrm{V}^{-1}\,\mathrm{s}^{-1}$ in Ga:ZnO (REFS[198,208])) and exhibit the lowest loss factors among doped semiconductors, with $\varepsilon_{co}'' \approx 0.15$. More recently, the development of various 2D semiconductor films such as silicene[212,213] and transition-metal dichalcogenides such as MoS_2 (REF.[214]) have driven advancements in electronics and optics, and offer new opportunities to explore NZI physics. For example, preliminary reports demonstrate that emerging chalcogenide materials may facilitate the creation of NZI and ENZ regions in the visible[215–217]. As a result of their exceptional tunability, well-developed fabrication methods and low optical losses, doped semiconductors are poised to continue driving NZI and ENZ research in the infrared spectral range.

Phononic materials. Phononic materials exhibit vibrational resonances that can give rise to a metallic region in the material[36,218]. Generally, this occurs between the resonant frequencies of the longitudinal and transverse optical phonons, a region called the reststrahlen band[192,219]. The effect can be modelled using the Lorentz formalism[218] (BOX 1) and provides a straightforward approach to achieving NZI and ENZ properties in the

Box 3 | Nonlinear dynamics in metal oxides

Transparent conductive oxides exhibit near-zero-index (NZI) enhanced nonlinearities. Here, we focus on intensity-dependent electron nonlinearities in which the probe photon resides at the NZI frequency, ω_{NZI}, and is modulated by a pump photon of frequency ω_p via an effective, third-order, nonlinear coefficient $\chi_{eff}^{(3)}(\omega_{NZI},\omega_p)$. Broadly speaking, the nonlinearities can be differentiated into two classes, depending on the relative energies of the bandgap and the optical pump. Intraband nonlinearities (panel **a** of the figure) occur when the energy of the optical pump is smaller than the bandgap of the semiconductor; conversely, interband nonlinearities (panel **b** of the figure) occur when the pump energy is greater than the bandgap. The experimentally observed quantity is the intensity-dependent refractive index $n(I)=n_o+n_2I$, where n_o is the base refractive index, I the intensity of the pump and n_2 the nonlinear refractive index. The nonlinear enhancement arises from the inverse proportional relation between the nonlinear refractive index and the base refractive index, $n_2 \propto \Delta\varepsilon/\sqrt{\varepsilon}$ (REFS[76,77]).

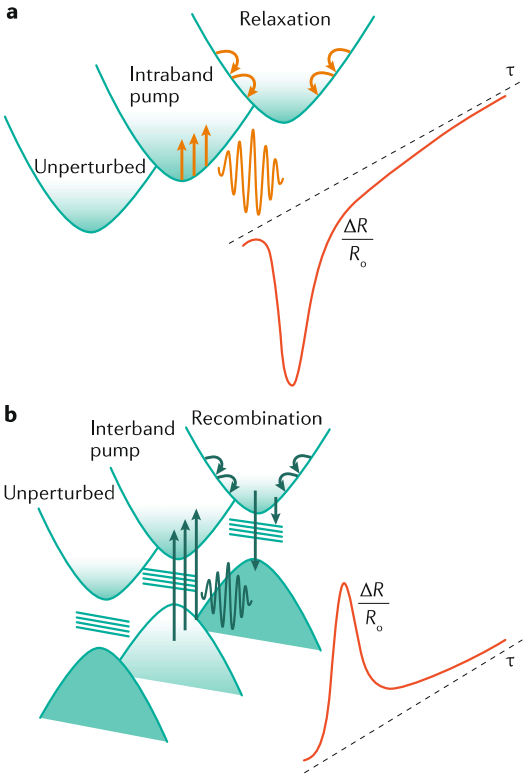

Intraband nonlinearities

When an ultrafast optical pulse with energy smaller than the bandgap excites a metal oxide, the conduction-band electrons undergo intraband transitions via free-carrier absorption. Before the pulse arrives, the conduction-band electrons are in equilibrium and described by a room-temperature Fermi distribution, in which the Fermi energy resides inside the conduction band. Immediately following excitation, the electrons are energized and their distribution is highly non-thermal; however, within a few femtoseconds, the excited plasma relaxes via electron–electron scattering to a smeared-electron distribution described by a quasi-Fermi distribution and an elevated electron temperature T_e. The result is an increase in the average effective mass of the electron sea, due to an overall shift to higher-energy, higher-mass states within a non-parabolic conduction band, thereby producing a red-shift of the Drude plasma frequency[238,284]:

$$\Delta\varepsilon(\omega) \propto \frac{Nq^2}{\varepsilon_o}\left(\frac{1}{m_{avg,e}}-\frac{1}{m_{avg,i}}\right)\frac{1}{\omega^2+i\Gamma\omega} \quad \text{(B3.1)}$$

where N is the electron density, q the electron charge, $m_{avg,e(i)}$ the average mass of the electron population in the excited (initial) distributions $m_{avg,e(i)}=m^*_{avg,e(i)}\,m_o$, ε_0 the vacuum permittivity, ω the frequency and Γ the damping factor. This tends to reduce the reflectivity, as the material appears more dielectric. The thermalized plasma then dissipates energy through electron–phonon interactions, increasing the lattice temperature T_l, until the system returns to its initial equilibrium state. The two-temperature model is a common method to describe the temperature dynamics of electrons and phonons[74,285,286]:

$$C_e(T_e)\frac{\partial T_e}{\partial t}=\frac{\partial}{\partial z}\left(\kappa\frac{\partial T_e}{\partial z}\right)-G(T_e-T_l)+H \quad \text{(B3.2)}$$

$$C_l(T_l)\frac{\partial T_l}{\partial t}=G(T_e-T_l) \quad \text{(B3.3)}$$

where C_e and C_l are the volumetric heat capacity of electrons and the lattice, respectively, κ is the thermal conductivity, G is the electron–phonon coupling constant and H is the spatial-temporal source term. More sophisticated models of the electron temperature consider non-thermal electrons, non-parabolic bands and local-field corrections[29,197,285,287,288]. However, carrier-scattering models may also be used to describe the relaxation process without the need for a temperature-based definition.

Interband nonlinearities

For optical pulse energies greater than the bandgap, the dominant contribution to ultrafast transients comes from interband transitions. Electrons that reside in the valence band are promoted into the conduction band and increase the total free-carrier density, blue-shifting the plasma frequency (panel **b**). This, in turn, tends to increase the reflection, as the material appears more metallic. Excited carriers then relax via a manifold of pathways, dictated by the electronic properties of the material, which include band-to-band, trap-assisted and Auger recombination[289]. The local temporal evolution of the excited free-carrier population, N, is captured using a first-order rate equation, from which the initial change in electron population can be calculated from the pump's local absorption, fluence, energy, and, under appropriate fluences, multi-photon cross sections as[290,291]:

$$\frac{dN}{dt}=-AN-BN^2-CN^3 \quad \text{(B3.4)}$$

where A, B and C are the monomolecular, bimolecular and Auger recombination coefficients, respectively. The subsequent change to the permittivity, assuming a Drude material, is:

$$\Delta\varepsilon(\omega)=-\frac{\Delta Nq^2}{m\varepsilon_o}\frac{1}{\omega^2+\Gamma\omega} \quad \text{(B3.5)}$$

where m is the electron mass m^*m_o, ΔN the change in carrier density, ω the probe frequency, ε_o the free-space permittivity, q the electron charge, and Γ the Drude damping rate[292]. Additional contributions, such as band filling, are neglected, because we consider probe frequencies near the crossover point, at which free-carrier absorption is dominant. The extremely fast recombination rate in metal oxides is attributed to the large density of mid-gap defect states, which enhance trap-assisted recombination and reduce the relaxation times to the sub-picosecond range[293–295].

infrared spectral range, as the effect occurs naturally in heteropolar semiconductors (such as AlN (REF.[220]), GaN (REF.[221]) and SiC (REF.[36])) and in some 2D materials, such as hexagonal boron nitride (hBN[222–225]). One of the key strengths of phononic materials lies in their exceptionally low losses at the crossover point. As a result, many phononic materials achieve not only ENZ but also deep NZI effects (FIG. 2, pentagons). SiC ($\lambda_{co} = 10{,}500$ nm, $\varepsilon_{co}'' = 0.3$)[226], InP ($\lambda_{co} = 6{,}500$ nm, $\varepsilon_{co}'' = 0.1$)[227] and hBN ($\lambda_{co} = 12{,}350$ nm, $\varepsilon_{co}'' = 0.05$)[225] are among the most promising materials in this class and can exhibit a refractive index several times closer to zero than other materials.

A key area of interest for phononic NZI and ENZ materials has been the study of ENZ and Berreman modes for coupled light–matter interactions. These modes exhibit unique, nearly flat dispersion at the permittivity crossover, which is useful for producing sharp, perfect-absorption resonant modes (BOX 2). Initial investigations focused on the coupling between planar metamaterials and doped semiconductor nanolayers at near-infrared and mid-infrared wavelengths[24,44,109]. A large Rabi splitting was observed in these systems because of the strong coupling between the metamaterial resonators and the ENZ mode of the nanolayers. Strong coupling between a single surface phonon polariton at a SiC/AlN interface with an ENZ phonon polariton in the ultrathin AlN film was recently demonstrated and shown to exhibit hybrid features of the constituent modes, namely, long propagation length and ultrahigh field confinement[228] (FIG. 3f).

Additionally, several theoretical works have illustrated the potential of phononic materials in the NZI regime[229]. For example, silicon carbide is a promising material for enhancing the spatial coherence of thermal radiation. When placing a thermal emitter inside the ENZ material cavity, the large phase velocity results in a nearly uniform phase across the cavity, enhancing coherence. However, when an additional resonant structure is included inside the cavity, such as a high-index rod or sphere[230], even for random excitations, the total emitted field is uniform in magnitude and phase on the surface with enhanced emission (FIG. 3g). Under these conditions, the emission pattern is determined by the shape of the cavity, allowing more efficient control of thermal radiation. This unique property of NZI films has been used for the design of selective thermal and mid-infrared emitters consisting of either ultrathin films of doped semiconductors or phononic materials to engineer the emissivity of thin-film stacks[220,231].

It has also been predicted that electric levitation using ENZ materials is achievable, because the electric field distribution is similar to the magnetic field distribution, which enables magnetic levitation with superconductors[232]. The electric field produced by an oscillating dipole placed near an ENZ medium would be parallel to the surface, as its normal component would go to zero due to the continuity of the normal electric displacement field (FIG. 3g). The resulting average force on the particle would be $F_{z,\mathrm{avg}} \propto \mathrm{Re}\left(\frac{\varepsilon_0 - \varepsilon_{\mathrm{sub}}}{\varepsilon_0 + \varepsilon_{\mathrm{sub}}}\right)\left(\frac{h}{\lambda}\right)^{-4} P_{dipole}$, where $\varepsilon_{\mathrm{sub}}$ is the permittivity of the ENZ substrate, h the distance between the dipole and the substrate, and P_{dipole} the radiated power of the dipole. As a result, for distances smaller than the wavelength, a net positive force would act on the particle. Although small, for radio frequencies, the distances and values associated with the levitation condition are achievable ($f = 1$ GHz, $I = 6$ A, $h = \lambda/100 \approx 3$ mm), should a suitable ENZ material be found. In the optical range, the small distances required introduce additional problems, such as the effects of van der Waals forces, Casimir forces and forces due to optical excitation of the emitter, which make the realization of electric levitation challenging.

Although the low losses of phononic materials are key for many applications, the high quality factor of phononic resonances ($Q \approx 200$ (REF.[219])) makes them particularly attractive for switching devices. However, the resonance occurs owing to vibrational modes within the material and it is difficult to statically tune the position of the NZI or ENZ point. The primary methods to tune the resonance are strain, thickness and control of the dielectric environment[219,233], but there are also methods to achieve dynamic control of the resonance[234]. Phononic materials are presently the best approximations of zero-index materials; thus, they provide a playground to test fundamental physical phenomena and the limits of light–matter interactions.

Interband materials. Another interesting and largely underexplored approach to achieve NZI and ENZ properties is with Lorentz-type resonances, such as interband transitions or intersubband transitions. As shown in BOX 1, on the blue side of a Lorentz resonance, the permittivity has a dip. This feature can result in an ENZ region for materials with a strong resonance and/or a low background permittivity. Because of these two requirements, such properties are largely expected to reside within the blue and ultraviolet region, where interband transitions are prevalent and the background permittivity of the host material is reduced. In fact, in $Bi_{1.5}Sb_{0.5}Te_{1.8}Se_{1.2}$, this effect was used to achieve plasmonic behaviour (negative permittivity) in the ultraviolet region[235]. Naturally, a permittivity crossover exists in this material as well, at 200 nm ($\varepsilon_{co}'' = 3$) and 660 nm ($\varepsilon_{co}'' = 26$).

Although an ENZ region can be found in interband materials, optical losses near the resonance constitute a challenge. As a result, achieving NZI effects is difficult. However, the ENZ region may be beneficial for enhancing optical absorption effects.

Nonlinear optics

All-optical control of materials properties and devices is one of the ultimate goals of photonics; however, photon–photon interactions are extraordinarily weak, so it becomes necessary to mediate them with matter. This is typically accomplished by utilizing inherent material nonlinearities. However, most light–matter interactions are linear and only exhibit a weak nonlinear response[236]. Large field amplitudes are, therefore, typically required to generate efficient, nonlinear light–matter interactions. Consequently, considerable efforts in nonlinear optics research are devoted to finding novel ways to enhance nonlinear effects or discovering or engineering new materials with a large nonlinear response. For example, large changes in transmission can be achieved using the

intensity-activated birefringence zero-crossing shift[237]. The effect exploits the iso-index point of a crystal (such as $CuAlSe_2$), at which the birefringence changes sign, giving rise to a wavelength for which the ordinary and extraordinary directions have the same index, so that polarization cross-coupling is possible. When the crystal is placed between crossed polarizers, a filter is formed whose transmission curve can be shifted by nonlinear modulation, resulting in strong modulation of the transmission.

Among the many approaches studied, NZI materials are intrinsically well suited for enhancing nonlinear optical interactions because of their small refractive index and the associated effects, such as diverging velocities, wavelength expansion and field confinement[238]. In the case of nonlinear optics, the efficiency of the process hinges on key elements such as phase matching and interaction length of the photons, as well as the peak electric field. NZI materials help to meet these conditions thanks to three properties: a diverging phase velocity (that is, a diverging wavelength), which ensures phase matching is satisfied (FIG. 4a); a slow group velocity, which causes light to spend more time inside the material, increasing the effective interaction length;

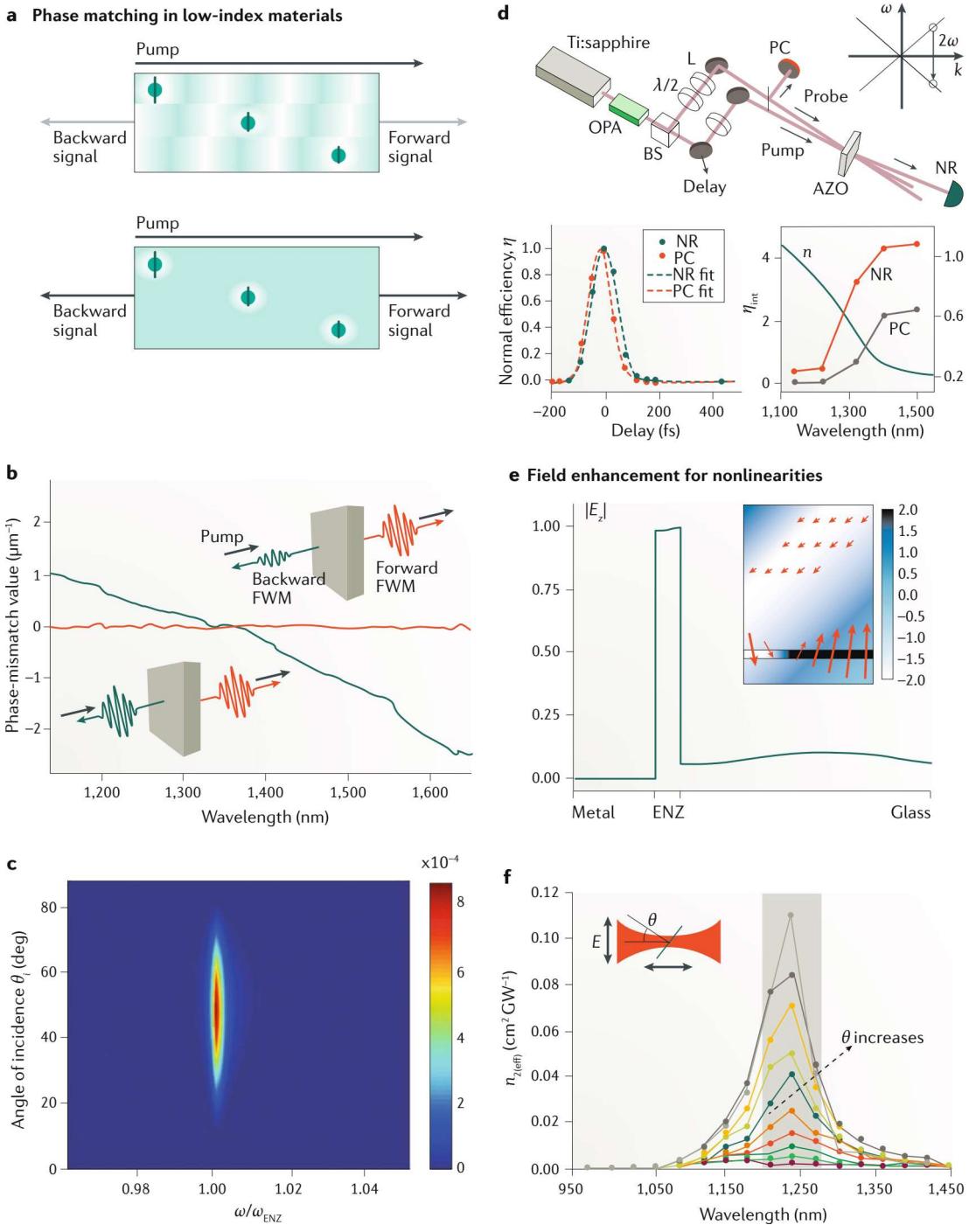

the continuity of the displacement field across the NZI interface, which results in an extremely large electric field within the NZI material for oblique illumination (FIG. 4b). As an example, we can consider the output intensity of a second-harmonic process proportional to $\frac{I^2L^2}{n_\omega^2 n_{2\omega}}\mathrm{sinc}(\frac{\Delta kL}{2})$. In this case, when the refractive index at the pump frequency (n_ω) tends to zero, the phase mismatch Δk tends to zero, such that $\mathrm{sinc}(x)\rightarrow 1$, while the group velocity is reduced, effectively increasing the interaction length L (I is the pump intensity). All these effects tend to increase the conversion efficiency of the nonlinear process, which is ultimately limited by the loss within the material. Similar arguments can be made for other nonlinear phenomena, such as four-wave mixing (FWM) and the intensity-dependent refractive index. The result of these enhancement mechanisms in NZI materials are interactions with contributions comparable to the linear response, as was shown in transparent conducting oxides[239]. These observations make NZI materials an exciting platform for investigating nonlinear optical phenomena.

Boosting nonlinearities using a uniform phase distribution and field enhancement in NZI materials can be done for both naturally occurring materials and artificially engineered structures. Waveguides operating at cut-off frequencies were among the first materials used to demonstrate remarkable nonlinear enhancements due to the uniform field and high confinement along the propagation direction[42,55]. When nonlinear elements are incorporated into a waveguide, a number of interesting nonlinear phenomena can be observed, such as efficient control of subwavelength tunnelling[23], low-threshold hysteresis and giant, second-order nonlinear signals[240]. Similar effects have been noted in other nanostructured materials, such as metamaterials[27,82,85,241–243] and photonic crystals[80]. More information can be found in the reviews in REFS[13,70,244]; here, we focus on nonlinearities occurring in homogeneous NZI and ENZ materials.

Fig. 4 | **Nonlinear optics in near-zero-index media. a** | Schematic of phase matching in a non-ϵ-near-zero (ENZ) medium (top) and in an ENZ medium (bottom). The phase variation is constant across the ENZ medium and contributes to both forward and backward signal generation. This can also be understood by considering the wave vector mismatch, which vanishes for a near-zero-index (NZI) material with $k_{pump}\rightarrow 0$. **b** | Enhanced backward four-wave mixing (FWM) in a fishnet metamaterial with a NZI wavelength near 1,360 nm. **c** | Second-harmonic generation enhancement in a low-loss silicon/Dy:CdO multilayer film. **d** | Observation of efficient phase conjugation (PC) and negative refraction (NR) in a thick film of aluminium-doped zinc oxide (AZO) near its NZI wavelength. The output of a Ti:sapphire laser is passed through an optical parametric amplifier (OPA) through a beam splitter (BS) to generate a pump and probe beam, in which the probe is passed through a lens (L) before arriving on the AZO sample. When the pump and probe arrive simultaneously, a peak in the PC and NR beams occurs, with a width limited to the temporal cross correlation width of the two pulses (bottom-left). The efficiency, η, of PC and NR generation coincides with the real index of the film, demonstrating the effect of the NZI condition (bottom-right). **e** | Field enhancement across an ENZ film sandwiched between a metal and a glass layer. The inset shows the electric field vector map for an oblique plane wave excitation (white shaded region) that couples to the ENZ film, producing a strong confinement and enhancement of the out-of-plane electric field. **f** | Kerr nonlinear coefficient, $n_{2(eff)}$, of an indium tin oxide film extracted using the Z-scan technique for a range of transverse magnetic-polarized incident angles (θ). The NZI region is shaded in grey. Panel **b** is reproduced with permission from REF.[27], AAAS. Panel **c** is adapted with permission from REF.[82], copyrighted by the American Physical Society. Panel **d** is adapted with permission from REF.[250], copyrighted by the American Physical Society. Panel **f** reproduced with permission from REF.[29], AAAS.

Frequency mixing. One of the most fundamental nonlinear processes is harmonic generation. Harmonic processes depend critically on the field intensity, interaction length and phase matching, and, therefore, benefit from NZI enhancements, as was predicted[65,245–248] and experimentally demonstrated[81,83,97]. For example, the second-harmonic generation (SHG) efficiency under off-normal illumination was compared for ITO thin films with a thickness of ~40 nm and varied permittivity crossover wavelengths (λ_{co} = 1,050–1,630 nm, $\varepsilon_{co}'' \approx 0.5$)[81]. In this condition, the NZI nature of the film aids phase matching and the off-axis illumination couples with quasi-Brewster modes in the ITO film to further enhance field confinement and interaction length. A peak in the SHG efficiency of the ITO layers was consistently found in the NZI region of each sample (which varied between 1,050 nm and 1,630 nm). Additionally, the magnitude of the SHG signal was comparable to that of the signal obtained from a 0.5-mm-thick crystalline quartz substrate[236], which implies an enhancement of the process of 4 orders of magnitude. Interestingly, TiN films with varying permittivity crossovers in the visible (λ_{co} = 510–645 nm, ε_{co}'' = 3–8), which coincides with the second harmonic, were also tested. No clear peak was observed at the permittivity crossover, indicating that the large losses in the system and the lack of enhancement at the pump frequency restricted the observable enhancement of the SHG signal. Similar avenues have also recently been used to enhance high-harmonic-generation processes[249].

It is also interesting to consider materials in which the NZI condition is realized only in one or two directions instead of in all directions, as in isotropic materials. Theoretical investigations of alternating silicon and dysprosium-doped cadmium oxide (Dy:CdO) 10-nm-thick layers (FIG. 4c) suggest that, in this system, SHG is enhanced by as much as a factor of 20 (total SHG efficiency of ~10^{-5}) in the NZI region compared to bulk Dy:CdO of the same overall thickness, and is comparable to that of conventional nonlinear materials[82]. This is attributed to the additional confinement provided by the anisotropy and is especially useful for boosting surface nonlinearities when the constituent materials do not possess an inherent bulk $\chi^{(2)}$.

With third-order nonlinearities, a rich set of potential frequency-mixing combinations is available through FWM processes. Because three input photons are involved, the efficiency is extremely sensitive to the phase-matching criteria and to the refraction index of the material. Thanks to the diverging wavelengths provided by NZI media, phase-matching criteria are greatly relaxed in these materials and all photons add coherently (FIG. 4a). In fact, enhanced third-harmonic generation was demonstrated in ITO layers, under similar conditions as those discussed above for SHG[97]. The third-harmonic generation in the NZI region was two orders of magnitude bigger than at wavelengths far from this region, and the total $\chi_{1111}^{(3)}$ was 600 times larger than in crystalline silicon.

Additionally, third-order nonlinearities allow for interesting processes such as phase conjugation, which implies a time-reversal of the wavefront. In the formal

demonstration of this process, two counter-propagating pump beams within the medium are used to provide equal and opposite momentum, such that the introduction of a third probe beam produces an output beam with opposite momentum to maintain momentum conservation; this beam is excited by the complex conjugate of the third beam[236]. However, phase conjugation was achieved in a 500-nm-thick, aluminium-doped zinc oxide (AZO) film without counter-propagating pumps and with an internal efficiency approaching unity[250]. The origination of the phase conjugation for this degenerate case, when pump and probe wavelengths are identical, is proposed to be the result of a time-dependent optical surface oscillating at the second harmonic of the pump, which modulates the probe beam, coupling two output beams, (k,ω) and $(k,-\omega)$, in the frequency–momentum space[251] (FIG. 4d). The result is the generation of a backwards-propagating phase-conjugate wave and of a forward-propagating wave with negative refraction; both were observed in the experiment with near-unity conversion efficiencies.

Intensity-dependent refractive index. The intensity-dependent modulation of the refractive index is another widely studied nonlinear effect in NZI materials (FIG. 4e). However, unlike frequency-mixing nonlinear processes, index modulation has predominately been achieved through effects such as free-carrier generation (interband) and absorption (intraband) processes (BOX 3). In fact, several works have demonstrated exceptionally large and ultrafast intensity-dependent index nonlinearities at NZI frequencies, particularly within films of metal oxides, such as the families of zinc[28,34,74,242], indium[29,76,77] and cadmium oxides[252], inducing effects such as metal-to-dielectric transitions[253], optical Doppler effect[78] and non-reciprocity[254].

Initial studies of index modulation in NZI materials included the observation of non-degenerate, free-carrier generation in AZO films[28]. Here, a material with initial index at the crossover $n = 0.5 + i0.2$ was modulated by $\Delta n = -0.17 + i0.25$ when excited with a 325-nm pump at normal incidence. The recombination time of the free carriers was found to be less than 100 fs, giving rise to an ultrafast and large change in the reflection and transmission of the film. Shortly thereafter, even larger nonlinear index modulation was observed in ITO films using a Z-scan technique through intraband processes[29]. As this measurement is inherently degenerate (as opposed to the non-degenerate pump–probe measurement in REF.[28]), both the pump and probe wavelengths reside within the NZI region and simultaneously experience enhancement. Consequently, degenerate processes scale as n_{pump}^{-2} compared with n_{pump}^{-1} for non-degenerate processes. Through spectral measurements, the nonlinear index modulation was shown to reach its peak in the NZI region, and off-axis illumination provided an additional boost. Overall, a sub-picosecond index modulation as large as $\Delta n \approx 0.7$ was observed, starting from an initial index at the crossover $n = 0.42 + i0.42$, more than doubling the refractive index of ITO (FIG. 4f).

More recently, NZI-enhanced interband and intraband processes have been combined in AZO films[74]. The refractive index changes between interband and intraband processes are opposite in sign, enabling unique opportunities for shaping the refractive index of a material in time and space. Using a two-colour pump–probe spectroscopy setup with a 262-nm (interband excitation) pump, a 787-nm (intraband excitation) pump and a 1,300-nm probe, the reflection and transmission of the sample were studied while varying the arrival time of both the 787-nm pump and the 1,300-nm probe. The results indicate that these sub-picosecond, nonlinear interactions are independent for pump fluences smaller than 10–20 mJ cm^{-2}, enabling the algebraic summation of the responses. This linearity is a key foundation for the development of many potentially useful devices realizing, for example, ultrafast pulse shaping, complex spatial index modulation, spectrum control and multi-state optical transmission.

It is important to note that these interband and intraband index modulation processes are proportional to $\Delta\varepsilon/\sqrt{\varepsilon}$, such that the minimization of the index is the key factor, not the real permittivity[76,77]. This is illustrated in a study of the nonlinear response of two sputtered TiN films, a polycrystalline film and a textured epitaxial film[255]. Under normal incidence, no enhancement to the nonlinear index coefficient was observed when passing through the ENZ region, likely due to the high loss within the material, which precludes NZI-based enhancement effects such as slow light. However, field confinement could still be achieved at oblique incidence due to boundary conditions and, when studied under off-axis illumination, a slight enhancement at the ENZ wavelength was observed for the granular epitaxial sample. This result illustrates the key role that loss and structural quality play on the enhancement of nonlinear effects, demonstrating that NZI conditions, rather than ENZ conditions, are the primary driver for nonlinear enhancement[29,76,77,178].

Discussion and outlook

A wide range of NZI and ENZ materials, homogeneous and structured, have been studied across the spectrum, from ultraviolet to infrared, opening the path for several interesting future directions of research. For many described materials (FIG. 2), higher losses are experienced for shorter crossover wavelengths. As a result, NZI materials are difficult to achieve in the visible spectrum, in which only select elemental metals with limited tunability can be used. Therefore, the development of tailorable NZI materials in the visible is key for the introduction of NZI effects in various applications, such as microscopy, imaging, quantum nanophotonics and chemical sensing. Additionally, it would be desirable to explore methods to extend the already broad NZI and ENZ region present in some NZI materials, such as metals. A relatively flat dispersion combined with ENZ effects may provide access to efficient broadband absorption without structuring. This may be accomplished through controlling the material's stoichiometry, alloying multiple materials with varied ENZ regions or by realizing ultrathin (few atomic layers) films with properties in between those of 2D and 3D materials, which are particularly sensitive to dynamic tuning methods, such

as electrical accumulation, optical modulation and mechanical stress and strain[144]. Furthermore, the discovery and investigation of new 2D and other van der Waals materials[219] are giving rise to a plethora of new exotic and coupled polariton modes in materials such as GaAs (REF.[35]) and black phosphorous[256]. Such materials may also give rise to dispersion conditions similar to those of bulk NZI and ENZ materials, which may provide new avenues for discovery.

We have emphasized the application of NZI materials for enhancing a broad range of nonlinear interactions. However, it should be noted that a key reason for the enhancement of nonlinear phenomena is the reduction of the group velocity observed in NZI materials[238]. Slow light can also be produced by several different approaches, such as photonic crystals, waveguides, random media and optical resonators. In fact, some of these methods can achieve slow-light effects with significantly lower loss than homogeneous NZI materials[61–63]. As a result, the structures can provide a narrow, high-Q-factor resonance and can produce appreciable changes in the optical properties in response to small perturbations ($\Delta n \approx 1\times10^{-3}$–$1\times10^{-2}$), which is useful for developing sensitive nonlinear sensors, switches and filters[66]. However, the large Q-factor and slow relaxation may make high-speed and broad-bandwidth applications challenging[257]. Alternatively, slow-light effect combined with the low-Q resonance in homogeneous NZI and ENZ materials can be useful for situations in which losses, broad enhancement bandwidth and local NZI effects are desired, such as in perfect absorption, optical-energy harvesting, absorption-driven nonlinear effects (such as free-carrier effects) and ultrafast, nonlinear devices. Although high-contrast switching in NZI materials requires a large change in the optical properties, or operation near a resonance (BOX 1), radical index modulations are possible ($\Delta n \approx 0.1$–1) and enable a shift of the crossover point by as much as ~100 nm (REFS[78,178]) and transitions between metallic and dielectric materials[253]. The combination of these properties of homogeneous NZI and ENZ materials with their simplicity of fabrication, good static tunability and broad wavelength coverage provides an avenue to enhance light–matter interactions in some, although not all, application spaces.

In transparent conducting oxides, both second-order and third-order nonlinear processes have shown remarkable efficiencies, and various applications are being actively pursued, including studies of adiabatic frequency conversion[78,178,258]. Furthermore, additional benefits may be found exploring other emerging optical materials, such as MXenes and doped nitride, carbide and phosphide semiconductor compounds. Another research direction is the use of hybrid NZI and ENZ materials with metamaterials or metasurfaces to further enhance optical effects. The recent demonstration of a record high refractive index and phase shift in a metasurface coupled to a thin ENZ layer has shown that the nonlinearity in an ENZ film can be further enhanced by plasmonic near-field coupling, which may have implications in quantum photonics[75].

Advancements should also be made in the theoretical description of the nonlinear enhancement in various NZI materials, such as heavily doped semiconductors. Specifically, the relationship between phenomenological (driven by free-carrier effects) and more standard perturbative expansion models (driven by nonlinear susceptibilities) is unclear, as is their applicability to various effects and applications. This is central to the ability of a model to predict or aid understanding[29,178,239]. In addition, it is likely that there is a significant, non-local contribution near the crossover wavelength, especially in ultrathin films supporting ENZ and Berreman modes, which has yet to be investigated. Hydrodynamic models that account for both nonlinear and non-local contributions in dilute plasmas could possibly provide deeper insight into these questions[127,246,259,260].

From the point of view of applications, NZI-enhanced nonlinearities represent a very exciting research direction. The large nonlinearities that have been observed in transparent conducting oxide NZI films could potentially enable extremely fast and efficient modulators for on-chip nanophotonic applications, in which ultra-small propagation lengths mitigate the inherent loss factor[29]; unlock fascinating avenues for modelling cosmological effects[261–263]; and enhance quantum interactions[25,73,264]. Combining NZI materials with resonant structures may be useful for the exploration of strong coupling, which may help to control emission and to further enhance the tunability of devices. Particularly, it would be interesting to explore NZI strong coupling in the context of Fano resonances, embedded eigenstates and bound states in the continuum[265] for photonic and plasmonic systems, in which losses as a function of coupling strength can be controlled[266–268]. In this sense, NZI materials are a unique platform to couple materials development with optical science and to advance both fundamental and application-driven research.

Published online: 26 September 2019

1. Ronchi, V. & Barocas, V. *Nature of Light: An Historical Survey* (Heinemann Educational Books, 1970).
2. Hecht, E. *Optics* (Pearson, 2017).
3. Yablonovitch, E. Inhibited spontaneous emission in solid-state physics and electronics. *Phys. Rev. Lett.* **58**, 2059–2062 (1987).
4. Joannopoulos, J. D., Johnson, S. G., Winn, J. N. & Meade, R. D. *Photonic Crystals: Molding the Flow of Light* (Princeton University Press, 2008).
5. Smith, D. R., Padilla, W. J., Vier, D. C., Nemat-Nasser, S. C. & Schultz, S. Composite medium with simultaneously negative permeability and permittivity. *Phys. Rev. Lett.* **84**, 4184–4187 (2000).
6. Ziolkowski, R. W. & Heyman, E. Wave propagation in media having negative permittivity and permeability. *Phys. Rev. E* **64**, 056625 (2001).
7. Elser, J., Wangberg, R., Podolskiy, V. A. & Narimanov, E. E. Nanowire metamaterials with extreme optical anisotropy. *Appl. Phys. Lett.* **89**, 261102 (2006).
8. Veselago, V. G. The electrodynamics of substances with simultaneously negative values of epsilon and mu. *Sov. Phys. Uspekhi* **10**, 509–514 (1968).
9. Pendry, J. Negative refraction makes a perfect lens. *Phys. Rev. Lett.* **85**, 3966–3969 (2000).
10. Shalaev, V. M. et al. Negative index of refraction in optical metamaterials. *Opt. Lett.* **30**, 3356–3358 (2005).
11. Jacob, Z., Alekseyev, L. V. & Narimanov, E. Optical hyperlens: far-field imaging beyond the diffraction limit. *Opt. Express* **14**, 8247–8256 (2006).
12. Zhang, F., Kang, L., Zhao, Q., Zhou, J. & Lippens, D. Magnetic and electric coupling effects of dielectric metamaterial. *New J. Phys.* **14**, 33031 (2012).
13. Urbas, A. M. et al. Roadmap on optical metamaterials. *J. Opt.* **18**, 093005 (2016).
14. Adams, D. C. et al. Funneling light through a subwavelength aperture with epsilon-near-zero materials. *Phys. Rev. Lett.* **107**, 133901 (2011).
15. Enoch, S., Tayeb, G., Sabouroux, P., Guérin, N. & Vincent, P. A metamaterial for directive emission. *Phys. Rev. Lett.* **89**, 213902 (2002).
16. Garcia, N., Ponizovskaya, E. V. & Xiao, J. Q. Zero permittivity materials: band gaps at the visible. *Appl. Phys. Lett.* **80**, 1120–1122 (2002).
17. Ziolkowski, R. W. Propagation in and scattering from a matched metamaterial having a zero index of refraction. *Phys. Rev. E* **70**, 046608 (2004).

18. Lovat, G., Burghignoli, P., Capolino, F., Jackson, D. R. & Wilton, D. R. Analysis of directive radiation from a line source in a metamaterial slab with low permittivity. *IEEE Trans. Antennas Propag.* **54**, 1017–1030 (2006).
19. Silveirinha, M. & Engheta, N. Tunneling of electromagnetic energy through subwavelength channels and bends using ε-near-zero materials. *Phys. Rev. Lett.* **97**, 157403 (2006).
20. Silveirinha, M. G. & Engheta, N. Theory of supercoupling, squeezing wave energy, and field confinement in narrow channels and tight bends using epsilon near-zero metamaterials. *Phys. Rev. B* **76**, 245109 (2007).
21. Alù, A., Silveirinha, M. G., Salandrino, A. & Engheta, N. Epsilon-near-zero metamaterials and electromagnetic sources: Tailoring the radiation phase pattern. *Phys. Rev. B* **75**, 155410 (2007).
22. Mahmoud, A. M. & Engheta, N. Wave–matter interactions in epsilon-and-mu-near-zero structures. *Nat. Commun.* **5**, 5638 (2014).
23. Powell, D. A. et al. Nonlinear control of tunneling through an epsilon-near-zero channel. *Phys. Rev. B* **79**, 245135 (2009).
24. Campione, S., Wendt, J. R., Keeler, G. A. & Luk, T. S. Near-infrared strong coupling between metamaterials and epsilon-near-zero modes in degenerately doped semiconductor nanolayers. *ACS Photonics* **3**, 293–297 (2016).
25. Liberal, I. & Engheta, N. Nonradiating and radiating modes excited by quantum emitters in open epsilon-near-zero cavities. *Sci. Adv.* **2**, e1600987 (2016).
26. Kim, J. et al. Role of epsilon-near-zero substrates in the optical response of plasmonic antennas. *Optica* **3**, 339–346 (2016).
27. Suchowski, H. et al. Phase mismatch–free nonlinear propagation in optical zero-index materials. *Science* **342**, 1223–1226 (2013).
28. Kinsey, N. et al. Epsilon-near-zero Al-doped ZnO for ultrafast switching at telecom wavelengths. *Optica* **2**, 616–622 (2015).
29. Alam, M. Z., De Leon, I. & Boyd, R. W. Large optical nonlinearity of indium tin oxide in its epsilon-near-zero region. *Science* **352**, 795–797 (2016).
30. Naik, G. V., Shalaev, V. M. & Boltasseva, A. Alternative plasmonic materials: beyond gold and silver. *Adv. Mater.* **25**, 3264–3294 (2013).
31. Wang, Y., Capretti, A. & Dal Negro, L. Wide tuning of the optical and structural properties of alternative plasmonic materials. *Opt. Mater. Express* **5**, 2415–2430 (2015).
32. Zhang, C. et al. High-performance doped silver films: overcoming fundamental material limits for nanophotonic applications. *Adv. Mater.* **29**, 1605177 (2017).
33. Naik, G. V., Kim, J. & Boltasseva, A. Oxides and nitrides as alternative plasmonic materials in the optical range. *Opt. Mater. Express* **1**, 1090–1099 (2011).
34. Tyborski, T. et al. Ultrafast nonlinear response of bulk plasmons in highly doped ZnO layers. *Phys. Rev. Lett.* **115**, 147401 (2015).
35. Streyer, W., Feng, K., Zhong, Y., Hoffman, A. J. J. & Wasserman, D. Engineering the reststrahlen band with hybrid plasmon/phonon excitations. *MRS Commun.* **6**, 1–8 (2016).
36. Caldwell, J. D. et al. Low-loss, extreme subdiffraction photon confinement via silicon carbide localized surface phonon polariton resonators. *Nano Lett.* **13**, 3690–3697 (2013).
37. Maas, R., Parsons, J., Engheta, N. & Polman, A. Experimental realization of an epsilon-near-zero metamaterial at visible wavelengths. *Nat. Photonics* **7**, 907–912 (2013).
38. Subramania, G., Fischer, A. J. & Luk, T. S. Optical properties of metal-dielectric based epsilon near zero metamaterials. *Appl. Phys. Lett.* **101**, 241107 (2012).
39. Basharin, A. A., Mavidis, C., Kafesaki, M., Economou, E. N. & Soukoulis, C. M. Epsilon near zero based phenomena in metamaterials. *Phys. Rev. B* **87**, 155130 (2013).
40. Li, Y. et al. On-chip zero-index metamaterials. *Nat. Photonics* **9**, 738–742 (2015).
41. Edwards, B., Alù, A., Young, M. E., Silveirinha, M. & Engheta, N. Experimental verification of epsilon-near-zero metamaterial coupling and energy squeezing using a microwave waveguide. *Phys. Rev. Lett.* **100**, 033903 (2008).
42. Vesseur, E. J. R., Coenen, T., Caglayan, H., Engheta, N. & Polman, A. Experimental verification of $n=0$ structures for visible light. *Phys. Rev. Lett.* **110**, 013902 (2013).
43. Campione, S., Brener, I. & Marquier, F. Theory of epsilon-near-zero modes in ultrathin films. *Phys. Rev. B* **91**, 121408 (2015).
44. Campione, S. et al. Epsilon-near-zero modes for tailored light-matter interaction. *Phys. Rev. Appl.* **4**, 044011 (2015).
45. Smolyaninov, I. I., Smolyaninova, V. N., Kildishev, A. V. & Shalaev, V. M. Anisotropic metamaterials emulated by tapered waveguides: application to optical cloaking. *Phys. Rev. Lett.* **102**, 213901 (2009).
46. Smolyaninova, V. N., Smolyaninov, I. I., Kildishev, A. V. & Shalaev, V. M. Experimental observation of the trapped rainbow. *Appl. Phys. Lett.* **96**, 211121 (2010).
47. Liu, R., Roberts, C. M., Zhong, Y., Podolskiy, V. A. & Wasserman, D. Epsilon-near-zero photonics wires. *ACS Photonics* **3**, 1045–1052 (2016).
48. Shcherbakov, M. R. et al. Ultrafast all-optical switching with magnetic resonances in nonlinear dielectric nanostructures. *Nano Lett.* **15**, 6985–6990 (2015).
49. Shorokhov, A. S. et al. Multifold enhancement of third-harmonic generation in dielectric nanoparticles driven by magnetic Fano resonances. *Nano Lett.* **16**, 4857–4861 (2016).
50. Kuznetsov, A. I., Miroshnichenko, A. E., Brongersma, M. L., Kivshar, Y. S. & Luk'yanchuk, B. Optically resonant dielectric nanostructures. *Science* **354**, aag2472 (2016).
51. Shcherbakov, M. R. et al. Enhanced third-harmonic generation in silicon nanoparticles driven by magnetic response. *Nano Lett.* **14**, 6488–6492 (2014).
52. Huang, X., Lai, Y., Hang, Z. H., Zheng, H. & Chan, C. T. Dirac cones induced by accidental degeneracy in photonic crystals and zero-refractive-index materials. *Nat. Mater.* **10**, 582–586 (2011).
53. Panoiu, N. C., Osgood, R. M. Jr., Zhang, S. & Brueck, S. R. J. Zero-n^- bandgap in photonic crystal superlattices. *J. Opt. Soc. Am. B* **23**, 506–513 (2006).
54. Hajian, H., Ozbay, E. & Caglayan, H. Enhanced transmission and beaming via a zero-index photonic crystal. *Appl. Phys. Lett.* **109**, 031105 (2016).
55. Reshef, O. et al. Direct observation of phase-free propagation in a silicon waveguide. *ACS Photonics* **4**, 2385–2389 (2017).
56. Vlasov, Y. A., O'Boyle, M., Hamann, H. F. & McNab, S. J. Active control of slow light on a chip with photonic crystal waveguides. *Nature* **438**, 65–69 (2005).
57. Marini, A. & García de Abajo, F. J. Self-organization of frozen light in near-zero-index media with cubic nonlinearity. *Sci. Rep.* **6**, 20088 (2016).
58. Ciattoni, A., Marini, A., Rizza, C., Scalora, M. & Biancalana, F. Polariton excitation in epsilon-near-zero slabs: transient trapping of slow light. *Phys. Rev. A* **87**, 053853 (2013).
59. D'Aguanno, G. et al. Frozen light in a near-zero index metasurface. *Phys. Rev. B* **90**, 054202 (2014).
60. Newman, W. D. et al. Ferrell–Berreman modes in plasmonic epsilon-near-zero media. *ACS Photonics* **2**, 2–7 (2015).
61. Javani, M. H. & Stockman, M. I. Real and imaginary properties of epsilon-near-zero materials. *Phys. Rev. Lett.* **117**, 107404 (2016).
62. Khurgin, J. B. Epsilon near zero materials vs. slow light and other resonance phenomena: anything new? (2017).
63. Khurgin, J. B. Epsilon near zero materials - photonics on steroids? (2018).
64. Moitra, P. et al. Realization of an all-dielectric zero-index optical metamaterial. *Nat. Photonics* **7**, 791–795 (2013).
65. Harris, S. E. & Hau, L. V. Nonlinear optics at low light levels. *Phys. Rev. Lett.* **82**, 4611–4614 (1999).
66. Khurgin, J. B. Slow light in various media: a tutorial. *Adv. Opt. Photonics* **2**, 287–318 (2010).
67. Luk, T. S. et al. Directional perfect absorption using deep subwavelength low-permittivity films. *Phys. Rev. B* **90**, 085411 (2014).
68. Lvovsky, A. I., Sanders, B. C. & Tittel, W. Optical quantum memory. *Nat. Photonics* **3**, 706–714 (2009).
69. Tsakmakidis, K. L., Boardman, A. D. & Hess, O. 'Trapped rainbow' storage of light in metamaterials. *Nature* **450**, 397–401 (2007).
70. Baba, T. Slow light in photonic crystals. *Nat. Photonics* **2**, 465–473 (2008).
71. Krauss, T. F. Why do we need slow light? *Nat. Photonics* **2**, 448–450 (2008).
72. Mahmoud, A. M., Liberal, I. & Engheta, N. Dipole-dipole interactions mediated by epsilon-and-mu-near-zero waveguide supercoupling [Invited]. *Opt. Mater. Express* **7**, 415–424 (2017).
73. Prain, A., Vezzoli, S., Westerberg, N., Roger, T. & Faccio, D. Spontaneous photon production in time-dependent epsilon-near-zero materials. *Phys. Rev. Lett.* **118**, 133904 (2017).
74. Clerici, M. et al. Controlling hybrid nonlinearities in transparent conducting oxides via two-colour excitation. *Nat. Commun.* **8**, 15829 (2017).
75. Alam, M. Z., Schulz, S. A., Upham, J., De Leon, I. & Boyd, R. W. Large optical nonlinearity of nanoantennas coupled to an epsilon-near-zero material. *Nat. Photonics* **12**, 79–83 (2018).
76. Benis, S., Zhao, P., Pattanaik, H. S., Hagan, D. J. & Van Stryland, E. W. Time-resolved nonlinear refraction of indium tin oxide at epsilon near zero. in *Conf. Lasers Electro-Optics* FM2F.2 https://doi.org/10.1364/CLEO_QELS.2017.FM2F.2 (OSA, 2017).
77. Benis, S., Hagan, D. J. & Van Stryland, E. W. Enhancement mechanism of nonlinear optical response of transparent conductive oxides at epsilon-near-zero. in *Conf. Lasers Electro-Optics* FF2E.1 https://doi.org/10.1364/CLEO_QELS.2018.FF2E.1 (OSA, 2018).
78. Shaltout, A. et al. Doppler-shift emulation using highly time-refracting TCO layer. in *Conf. Lasers Electro-Optics* FF2D.6 https://doi.org/10.1364/CLEO_QELS.2016.FF2D.6 (OSA, 2016).
79. Ciattoni, A. et al. Enhanced nonlinear effects in pulse propagation through epsilon-near-zero media. *Laser Photon. Rev.* **10**, 517–525 (2016).
80. Mattiucci, N., Bloemer, M. J. & D'Aguanno, G. Phase-matched second harmonic generation at the Dirac point of a 2-D photonic crystal. *Opt. Express* **22**, 6381–6390 (2014).
81. Capretti, A., Wang, Y., Engheta, N. & Dal Negro, L. Comparative study of second-harmonic generation from epsilon-near-zero indium tin oxide and titanium nitride nanolayers excited in the near-infrared spectral range. *ACS Photonics* **2**, 1584–1591 (2015).
82. Vincenti, M. A. et al. Second-harmonic generation in longitudinal epsilon-near-zero materials. *Phys. Rev. B* **96**, 045438 (2017).
83. Luk, T. S. et al. Enhanced third harmonic generation from the epsilon-near-zero modes of ultrathin films. *Appl. Phys. Lett.* **106**, 151103 (2015).
84. Marcos, J. S., Silveirinha, M. G. & Engheta, N. μ-near-zero supercoupling. *Phys. Rev. B* **91**, 195112 (2015).
85. Edwards, B., Alù, A., Silveirinha, M. G. & Engheta, N. Reflectionless sharp bends and corners in waveguides using epsilon-near-zero effects. *J. Appl. Phys.* **105**, 044905 (2009).
86. Iyer, P. P., Pendharkar, M., Palmstrøm, C. J. & Schuller, J. A. Ultrawide thermal free-carrier tuning of dielectric antennas coupled to epsilon-near-zero substrates. *Nat. Commun.* **8**, 472 (2017).
87. Schulz, S. A. et al. Optical response of dipole antennas on an epsilon-near-zero substrate. *Phys. Rev. A* **93**, 063846 (2016).
88. Liberal, I., Mahmoud, A. M. & Engheta, N. Geometry-invariant resonant cavities. *Nat. Commun.* **7**, 10989 (2016).
89. Mahmoud, A. M. & Engheta, N. "Static" optics. *arXiv* **1407**, 2338 (2014).
90. Cheng, D. *Field and Wave Electromagnetics*. (Addison-Wesley, 1983).
91. Reines, I. C., Wood, M. G., Luk, T. S., Serkland, D. K. & Campione, S. Compact epsilon-near-zero silicon photonic phase modulators. *Opt. Express* **26**, 21594–21605 (2018).
92. Kinsey, N., Ferrera, M., Shalaev, V. M. & Boltasseva, A. Examining nanophotonics for integrated hybrid systems: a review of plasmonic interconnects and modulators using traditional and alternative materials [Invited]. *J. Opt. Soc. Am. B* **32**, 121–142 (2015).
93. Sun, S., Badawy, A.-H. A., Narayana, V., El-Ghazawi, T. & Sorger, V. J. The case for hybrid photonic plasmonic interconnects (HyPPIs): low-latency energy-and-area-efficient on-chip interconnects. *IEEE Photonics J.* **7**, 1–14 (2015).
94. Sorger, V. J. et al. Experimental demonstration of low-loss optical waveguiding at deep sub-wavelength scales. *Nat. Commun.* **2**, 331 (2011).
95. Wang, C., Zhang, M., Stern, B., Lipson, M. & Lončar, M. Nanophotonic lithium niobate electro-optic modulators. *Opt. Express* **26**, 1547–1555 (2018).
96. Kinsey, N. et al. Practical platform for nanophotonics with refractory plasmonic metal nitrides and transparent conducting oxides. in Front. Opt. FM1B.3 https://doi.org/10.1364/FIO.2015.FM1B.3 (OSA, 2015).
97. Capretti, A., Wang, Y., Engheta, N. & Dal Negro, L. Enhanced third-harmonic generation in Si-compatible epsilon-near-zero indium tin oxide nanolayers. *Opt. Lett.* **40**, 1500–1503 (2015).

98. Liberal, I. & Engheta, N. Near-zero refractive index photonics. *Nat. Photonics* **11**, 149–158 (2017).
99. Sorger, V. J., Lanzillotti-Kimura, N. D., Ma, R. & Zhang, X. Ultra-compact silicon nanophotonic modulator with broadband response. *Nanophotonics* **1**, 17–22 (2012).
100. Lee, H. W. et al. Nanoscale conducting oxide PlasMOStor. *Nano Lett.* **14**, 6463–6468 (2014).
101. Babicheva, V. E. et al. Towards CMOS-compatible nanophotonics: Ultra-compact modulators using alternative plasmonic materials. *Opt. Express* **21**, 27326–27337 (2013).
102. Melikyan, A. et al. Surface plasmon polariton absorption modulator. *Opt. Express* **19**, 8855–8869 (2011).
103. Babicheva, V. E., Boltasseva, A. & Lavrinenko, A. V. Transparent conducting oxides for electro-optical plasmonic modulators. *Nanophotonics* **4**, 165–185 (2015).
104. Feigenbaum, E., Diest, K. & Atwater, H. A. Unity-order index change in transparent conducting oxides at visible frequencies. *Nano Lett.* **10**, 2111–2116 (2010).
105. Park, J., Kang, J. H., Liu, X. X. & Brongersma, M. L. Electrically tunable epsilon-near-zero (ENZ) metafilm absorbers. *Sci. Rep.* **5**, 15754 (2015).
106. Muskens, O. L. Extreme scattering and extraordinary nonlinearities of light in complex media. in *EOS Topical Meeting on Waves in Complex Photonics Media: Fundamentals and Device Applications 2018*. (EOS, 2018).
107. Strudley, T., Zehender, T., Blejean, C., Bakkers, E. P. A. M. & Muskens, O. L. Mesoscopic light transport by very strong collective multiple scattering in nanowire mats. *Nat. Photonics* **7**, 413–418 (2013).
108. Strudley, T. et al. Observation of intensity statistics of light transmitted through 3D random media. *Opt. Lett.* **39**, 6347–6350 (2014).
109. Jun, Y. C. et al. Epsilon-near-zero strong coupling in metamaterial-semiconductor hybrid structures. *Nano Lett.* **13**, 5391–5396 (2013).
110. Abb, M., Sepulveda, B., Chong, H. M. H. & Muskens, O. L. Transparent conducting oxides for active hybrid metamaterial devices. *J. Opt.* **14**, 114007 (2012).
111. Ma, Z., Li, Z., Liu, K., Ye, C. & Sorger, V. J. Indium-tin-oxide for high-performance electro-optic modulation. *Nanophotonics* **4**, 198–213 (2015).
112. Keeler, G. A. *et al*. Multi-gigabit operation of a compact, broadband modulator based on ENZ confinement in indium oxide. in *Opt. Fiber Commun. Conf.* Th3I.1 (IEEE, 2017).
113. Boyd, R. W. Slow and fast light: fundamentals and applications. *J. Mod. Opt.* **56**, 1908–1915 (2009).
114. Liberal, I. & Engheta, N. The rise of near-zero-index technologies. *Science* **358**, 1540–1541 (2017).
115. Werner, W. S. M., Glantschnig, K. & Ambrosch-Draxl, C. Optical constants and inelastic electron-scattering data for 17 elemental metals. *J. Phys. Chem. Ref. Data* **38**, 1013–1092 (2009).
116. Roberts, S. Optical properties of copper. *Phys. Rev.* **118**, 1509–1518 (1960).
117. Johnson, P. & Christy, R. Optical constants of transition metals: Ti, V, Cr, Mn, Fe, Co, Ni, and Pd. *Phys. Rev. B* **9**, 5056–5070 (1974).
118. Rakić, A. D. Algorithm for the determination of intrinsic optical constants of metal films: application to aluminum. *Appl. Opt.* **34**, 4755–4767 (1995).
119. Johnson, P. B. & Christy, R. W. Optical constants of the noble metals. *Phys. Rev. B* **6**, 4370–4379 (1972).
120. McMahon, J. M., Schatz, G. C. & Gray, S. K. Plasmonics in the ultraviolet with the poor metals Al, Ga, In, Sn, Tl, Pb, and Bi. *Phys. Chem. Chem. Phys.* **15**, 5415–5423 (2013).
121. Bloembergen, N., Burns, W. K. & Matsuoka, M. Reflected third harmonic generated by picosecond laser pulses. *Opt. Commun.* **1**, 195–198 (1969).
122. Smith, D. D. et al. *z*-Scan measurement of the nonlinear absorption of a thin gold film. *J. Appl. Phys.* **86**, 6200 (1999).
123. Marini, A. et al. Ultrafast nonlinear dynamics of surface plasmon polaritons in gold nanowires due to the intrinsic nonlinearity of metals. *New J. Phys.* **15**, 013033 (2013).
124. Boyd, R. W., Shi, Z. & De Leon, I. The third-order nonlinear susceptibility of gold. *Opt. Commun.* **326**, 74–79 (2014).
125. Moaied, M., Yajadda, M. M. A. & Ostrikov, K. Quantum effects of nonlocal plasmons in epsilon-near-zero properties of a thin gold film slab. *Plasmon.* **10**, 1615–1623 (2015).
126. David, C., Mortensen, N. A. & Christensen, J. Perfect imaging, epsilon-near zero phenomena and waveguiding in the scope of nonlocal effects. *Sci. Rep.* **3**, 2526 (2013).
127. Raza, S., Christensen, T., Wubs, M., Bozhevolnyi, S. I. & Mortensen, N. A. Nonlocal response in thin-film waveguides: Loss versus nonlocality and breaking of complementarity. *Phys. Rev. B* **88**, 115401 (2013).
128. Chalabi, H., Schoen, D. & Brongersma, M. L. Hot-electron photodetection with a plasmonic nanostripe antenna. *Nano Lett.* **14**, 1374–1380 (2014).
129. Hou, B., Shen, L., Shi, H., Kapadia, R. & Cronin, S. B. Hot electron-driven photocatalytic water splitting. *Phys. Chem. Chem. Phys.* **19**, 2877–2881 (2017).
130. Juan, M. L., Righini, M. & Quidant, R. Plasmon nano-optical tweezers. *Nat. Photonics* **5**, 349–356 (2011).
131. Juan, M. L., Gordon, R., Pang, Y., Eftekhari, F. & Quidant, R. Self-induced back-action optical trapping of dielectric nanoparticles. *Nat. Phys.* **5**, 915–919 (2009).
132. Ndukaife, J. et al. Long-range and rapid transport of individual nano-objects by a hybrid electrothermoplasmonic nanotweezer. *Nat. Nanotechnol* **11**, 53–59 (2016).
133. Qian, H., Xiao, Y. & Liu, Z. Giant Kerr response of ultrathin gold films from quantum size effect. *Nat. Commun.* **7**, 13153 (2016).
134. Zhu, F. et al. Epitaxial growth of two-dimensional stanene. *Nat. Mater.* **14**, 1020–1025 (2015).
135. Chaudhary, R. P., Saxena, S. & Shukla, S. Optical properties of stanene. *Nanotechnology* **27**, 495701 (2016).
136. Liao, M. et al. Superconductivity in few-layer stanene. *Nat. Phys.* **14**, 344–348 (2018).
137. Mannix, A. J. et al. Synthesis of borophenes: anisotropic, two-dimensional boron polymorphs. *Science* **350**, 1513–1516 (2015).
138. Sundararaman, R. et al. Plasmonics in Argentene. *arXiv* **1806**, 02672 (2018).
139. Zang, Y. et al. Realizing an epitaxial decorated stanene with an insulating bandgap. *Adv. Funct. Mater.* **28**, 1802723 (2018).
140. Khurgin, J. B. & Sun, G. In search of the elusive lossless metal. *Appl. Phys. Lett.* **96**, 181102 (2010).
141. Peña-Rodríguez, O. et al. Optical properties of Au-Ag alloys: an ellipsometric study. *Opt. Mater. Express* **4**, 403–410 (2014).
142. Weiss, D. E. & Muldawer, L. Optical properties of gold and dilute gold-zinc alloys. *Phys. Rev. B* **10**, 2254–2261 (1974).
143. Irani, G. B., Huen, T. & Wooten, F. Optical properties of gold and α-phase gold-aluminum alloys. *Phys. Rev. B* **6**, 2904–2909 (1972).
144. Boltasseva, A. & Shalaev, V. M. Transdimensional photonics. *ACS Photonics* **6**, 1–3 (2019).
145. Soref, R., Peale, R. E. & Buchwald, W. Longwave plasmonics on doped silicon and silicides. *Opt. Express* **16**, 6507–6514 (2008).
146. Cleary, J. W. et al. IR permittivities for silicides and doped silicon. *J. Opt. Soc. Am. B* **27**, 730–734 (2010).
147. Cleary, J. W. et al. Silicides for infrared surface plasmon resonance biosensors. *MRS Proc.* **1133-AA10-03** (2008).
148. Hu, J. et al. Evolutionary design and prototyping of single crystalline titanium nitride lattice optics. *ACS Photonics* **4**, 606–612 (2017).
149. Patsalas, P., Kalfagiannis, N. & Kassavetis, S. Optical properties and plasmonic performance of titanium nitride. *Materials* 8, 3128–3154 (2015).
150. Zgrabik, C. M. & Hu, E. L. Optimization of sputtered titanium nitride as a tunable metal for plasmonic applications. *Opt. Mater. Express* **5**, 2786–2797 (2015).
151. Gui, L. et al. Nonlinear refractory plasmonics with titanium nitride nanoantennas. *Nano Lett.* **16**, 5708–5713 (2016).
152. Smith, E. M. et al. Palladium germanides for mid- and long-wave infrared plasmonics. *MRS Adv.* **2**, 2385–2390 (2017).
153. Cleary, J. W. et al. Platinum germanides for mid- and long-wave infrared plasmonics. *Opt. Express* **23**, 3316–3326 (2015).
154. Strohfeldt, N. et al. Yttrium hydride nanoantennas for active plasmonics. *Nano Lett.* **14**, 1140–1147 (2014).
155. Babicheva, V. E. et al. CMOS compatible ultra-compact modulator. in *Conf. Lasers Electro-Optics* FTu3K.3 https://doi.org/10.1364/CLEO_QELS.2014.FTu3K.3 (2014).
156. Kinsey, N. et al. Effective third-order nonlinearities in metallic refractory titanium nitride thin films. *Opt. Mater. Express* **5**, 2395–2403 (2015).
157. Catellani, A. & Calzolari, A. Plasmonic properties of refractory titanium nitride. *Phys. Rev. B* **95**, 115145 (2017).
158. Dutta, A. et al. Plasmonic interconnects using zirconium nitride. in *Conf. Lasers Electro-Optics* JW2A.86 https://doi.org/10.1364/CLEO_AT.2016.JW2A.86 (2016).
159. Li, W. et al. Refractory plasmonics with titanium nitride: broadband metamaterial absorber. *Adv. Mater.* **26**, 7959–7965 (2014).
160. Kumar, M., Umezawa, N., Ishii, S. & Nagao, T. Examining the performance of refractory conductive ceramics as plasmonic materials: A theoretical approach. *ACS Photonics* **3**, 43–50 (2016).
161. Vertchenko, L., Akopian, N. & Lavrinenko, A. V. Epsilon-near-zero quantum networks. (2018).
162. Vertchenko, L., Akopian, N. & Lavrinenko, A. V. Epsilon-near-zero systems for quantum optics applications. in *Conf. Lasers Electro-Optics* FM4J.1 https://doi.org/10.1364/CLEO_QELS.2018.FM4J.1 (OSA, 2018).
163. Maurer, P. C. et al. Room-temperature quantum bit memory exceeding one second. *Science* **336**, 1283–1286 (2012).
164. Braic, L. et al. Titanium oxynitride thin films with tunable double epsilon-near-zero behavior for nanophotonic applications. *ACS Appl. Mater. Interfaces* **9**, 29857–29862 (2017).
165. Kumar, M., Ishii, S., Umezawa, N. & Nagao, T. Band engineering of ternary metal nitride system $Ti_{1-x}Zr_xN$ for plasmonic applications. *Opt. Mater. Express* **6**, 29–38 (2016).
166. Naldoni, A. et al. Solar-powered plasmon-enhanced heterogeneous catalysis. *Nanophotonics* **5**, 112–133 (2016).
167. Naldoni, A. et al. Broadband hot-electron collection for solar water splitting with plasmonic titanium nitride. *Adv. Opt. Mater.* **5**, 1601031 (2017).
168. Choi, S. K. et al. Photoelectrochemical hydrogen production on silicon microwire arrays overlaid with ultrathin titanium nitride. *J. Mater. Chem. A* **4**, 14008–14016 (2016).
169. Noginov, M. A. et al. Transparent conductive oxides: plasmonic materials for telecom wavelengths. *Appl. Phys. Lett.* **99**, 021101 (2011).
170. Gordon, T. R. et al. Shape-dependent plasmonic response and directed self-assembly in a new semiconductor building block, indium-doped cadmium oxide (ICO). *Nano Lett.* **13**, 2857–2863 (2013).
171. Li, S. Q. et al. Infrared plasmonics with indium-tin-oxide nanorod arrays. *ACS Nano* **5**, 9161–9170 (2011).
172. Wetterau, L. et al. Characterization of highly-doped GaN as a new material for plasmonic applications. in *Int. Conf. Optical MEMS Nanophotonics* 1–2 https://doi.org/10.1109/OMN.2016.7565937 (IEEE, 2016).
173. Hageman, P. R., Schaff, W. J., Janinski, J. & Liliental-Weber, Z. n-type doping of wurtzite GaN with germanium grown with plasma-assisted molecular beam epitaxy. *J. Cryst. Growth* **267**, 123–128 (2004).
174. Law, S., Adams, D. C., Taylor, A. M. & Wasserman, D. Mid-infrared designer metals. *Opt. Express* **20**, 12155–12165 (2012).
175. Kim, J. et al. Optical properties of gallium-doped zinc oxide — a low-loss plasmonic material: first-principles theory and experiment. *Phys. Rev. X* **3**, 041037 (2013).
176. Sachet, E. et al. Dysprosium-doped cadmium oxide as a gateway material for mid-infrared plasmonics. *Nat. Mater.* **14**, 414–420 (2015).
177. Tice, D. B. et al. Ultrafast modulation of the plasma frequency of vertically aligned indium tin oxide rods. *Nano Lett.* **14**, 1120–1126 (2014).
178. Caspani, L. et al. Enhanced nonlinear refractive index in ε-near-zero materials. *Phys. Rev. Lett.* **116**, 233901 (2016).
179. Wood, M. G. et al. Gigahertz speed operation of epsilon-near-zero silicon photonic modulators. *Optica* **5**, 233–236 (2018).
180. Hoessbacher, C. et al. The plasmonic memristor: a latching optical switch. *Opt. Quantum Electron.* **1**, 198–202 (2014).
181. Liu, K., Ye, C. R., Khan, S. & Sorger, V. J. Review and perspective on ultrafast wavelength-size electro-optic modulators. *Laser Photon. Rev.* **9**, 172–194 (2015).
182. DeVault, C. T. et al. Suppression of near-field coupling in plasmonic antennas on epsilon-near-zero substrates. *Optica* **5**, 1557–1563 (2018).
183. Huang, Y.-W. et al. Gate-tunable conducting oxides metasurfaces. *Nano Lett.* **16**, 5319–5325 (2016).
184. Howes, A., Wang, W., Kravchenko, I. & Valentine, J. Dynamic transmission control based on all-dielectric Huygens metasurfaces. *Optica* **5**, 787–792 (2018).

185. Kafaie Shirmanesh, G., Sokhoyan, R., Pala, R. A. & Atwater, H. A. Dual-gated active metasurface at 1550 nm with wide (>300°) phase tunability. *Nano Lett.* **18**, 2957–2963 (2018).
186. Ferrera, M. et al. Dynamic nanophotonics [Invited]. *J. Opt. Soc. Am. B* **34**, 95–103 (2017).
187. Campione, S., de Ceglia, D., Vincenti, M. A., Scalora, M. & Capolino, F. Electric field enhancement in ε-near-zero slabs under TM-polarized oblique incidence. *Phys. Rev. B* **87**, 035120 (2013).
188. Campione, S., Kim, I., de Ceglia, D., Keeler, G. A. & Luk, T. S. Experimental verification of epsilon-near-zero plasmon polariton modes in degenerately doped semiconductor nanolayers. *Opt. Express* **24**, 18782–18789 (2016).
189. Anopchenko, A., Tao, L., Arndt, C. & Lee, H. W. H. Field-effect tunable and broadband epsilon-near-zero perfect absorbers with deep subwavelength thickness. *ACS Photonics* **5**, 2631–2637 (2018).
190. Kalusniak, S., Sadofev, S. & Henneberger, F. ZnO as a tunable metal: new types of surface plasmon polaritons. *Phys. Rev. Lett.* **112**, 137401 (2014).
191. Streyer, W., Law, S., Rooney, G., Jacobs, T. & Wasserman, D. Strong absorption and selective emission from engineered metals with dielectric coatings. *Opt. Express* **21**, 9113–9122 (2013).
192. Zhong, Y., Malagari, S. D., Hamilton, T. & Wasserman, D. Review of mid-infrared plasmonic materials. *J. Nanophotonics* **9**, 093791 (2015).
193. De Vault, C. *et al*. Plasmonic antenna resonance pinning and suppression of near-field coupling from epsilon-near-zero substrate. in *Conf. Lasers Electro-Optics* FTu4H.5 https://doi.org/10.1364/CLEO_QELS.2017.FTu4H.5 (OSA, 2017).
194. Benz, A., Montaño, I., Klem, J. F. & Brener, I. Tunable metamaterials based on voltage controlled strong coupling. *Appl. Phys. Lett.* **103**, 263116 (2013).
195. Geiser, M., Scalari, G., Castellano, F., Beck, M. & Faist, J. Room temperature terahertz polariton emitter. *Appl. Phys. Lett.* **101**, 141118 (2012).
196. Kim, J., Naik, G., Emani, N., Guler, U. & Boltasseva, A. Plasmonic resonances in nanostructured transparent conducting oxide films. *IEEE J. Sel. Top. Quantum Electron.* **19**, 4601907 (2013).
197. Guo, P., Schaller, R. d., Ketterson, J. B. & Chang, R. P. H. Ultrafast switching of tunable infrared plasmons in indium tin oxide nanorod arrays with large absolute amplitude. *Nat. Photonics* **10**, 267–273 (2016).
198. Liu, H., Avrutin, V., Izyumskaya, N., Özgür, Ü. & Morkoç, H. Transparent conducting oxides for electrode applications in light emitting and absorbing devices. *Superlattices Microstruct.* **48**, 458–484 (2010).
199. Nomura, K. et al. Room-temperature fabrication of transparent flexible thin-film transistors using amorphous oxide semiconductors. *Nature* **432**, 488–492 (2004).
200. Schmidt, H. et al. Efficient semitransparent inverted organic solar cells with indium tin oxide top electrode. *Appl. Phys. Lett.* **94**, 243302 (2009).
201. Levy, D. H., Scuderi, A. C. & Irving, L. M. Methods of making thin film transistors comprising zinc-oxide-based semiconductor materials and transistors made thereby. US Patent US 2008/0299771 A1 (2007).
202. Li, Y. & Ong, B. S. Thin film transistor using an oriented zinc oxide layer. EU Patent EP1921681 A (2008).
203. Pinarbasi, M. & Freitag, J. Method of forming transparent zinc oxide layers for high efficiency photovoltaic cells. US Patent 12/616,578 (2009).
204. Li, X. et al. InGaN based light emitting diodes with Ga doped ZnO as transparent conducting oxide. *Phys. Status Solidi* **207**, 1993–1996 (2010).
205. Gorjanc, T. C., Leong, D., Py, C. & Roth, D. Room temperature deposition of ITO using r.f. magnetron sputtering. *Thin Solid Films* **413**, 181–185 (2002).
206. Frolich, A. & Wegener, M. Spectroscopic characterization of highly doped ZnO films grown by atomic-layer deposition for three-dimensional infrared metamaterials. *Opt. Mater. Express* **1**, 883–889 (2011).
207. Pradhan, A. K. et al. Extreme tunability in aluminum doped zinc oxide plasmonic materials for near-infrared applications. *Sci. Rep.* **4**, 6415 (2014).
208. Liu, H. Y. et al. Highly conductive and optically transparent GZO films grown under metal-rich conditions by plasma assisted MBE. *Phys. Status Solidi* **4**, 70–72 (2010).
209. Morkoç, H. & Özgür, Ü. *Zinc Oxide: Fundamentals, Materials and Device Technology*. (John Wiley & Sons, 2008).
210. Wang, A. et al. Indium-cadmium-oxide films having exceptional electrical conductivity and optical transparency: clues for optimizing transparent conductors. *Proc. Natl. Acad. Sci. USA* **98**, 7113–7116 (2001).
211. Kelley, K. P., Sachet, E., Shelton, C. T. & Maria, J.-P. High mobility yttrium doped cadmium oxide thin films. *APL Mater.* **5**, 076105 (2017).
212. Vogt, P. et al. Silicene: compelling experimental evidence for graphenelike two-dimensional silicon. *Phys. Rev. Lett.* **108**, 155501 (2012).
213. Zhao, J. et al. Rise of silicene: A competitive 2D material. *Prog. Mater. Sci.* **83**, 24–151 (2016).
214. Wang, Q. H., Kalantar-Zadeh, K., Kis, A., Coleman, J. N. & Strano, M. S. Electronics and optoelectronics of two-dimensional transition metal dichalcogenides. *Nat. Nanotechnol.* **7**, 699–712 (2012).
215. Krishnamoorthy, H. N. S., Gholipour, B., Zheludev, N. I. & Soci, C. A non-volatile chalcogenide switchable hyperbolic metamaterial. *Adv. Opt. Mater.* **6**, 1800332 (2018).
216. Piccinotti, D. et al. Tuneable Epsilon-Near-Zero in Chalcogenides. in *Metamaterials* 1–3 (2017).
217. Piccinotti, D. et al. Extraordinary Properties of Epsilon-Near-Zero and Low-Index Chalcogenide Metamaterials. in *Conf. Lasers Electro-Optics* FTh4H.6 (OSA, 2018).
218. Fox, M. *Optical Properties of Solids* (Oxford University Press, 2010).
219. Basov, D. N., Fogler, M. M. & García de Abajo, F. J. Polaritons in van der Waals materials. *Science* **354**, aag1992 (2016).
220. Nordin, L. et al. Mid-infrared epsilon-near-zero modes in ultra-thin phononic films. *Appl. Phys. Lett.* **111**, 091105 (2017).
221. Feng, K. et al. Localized surface phonon polariton resonances in polar gallium nitride. *Appl. Phys. Lett.* **107**, 081108 (2015).
222. Dai, S. et al. Tunable phonon polaritons in atomically thin van der Waals crystals of boron nitride. *Science* **343**, 1125–1129 (2014).
223. Yoxall, E. et al. Direct observation of ultraslow hyperbolic polariton propagation with negative phase velocity. *Nat. Photonics* **9**, 674–678 (2015).
224. Li, P. et al. Hyperbolic phonon-polaritons in boron nitride for near-field optical imaging and focusing. *Nat. Commun.* **6**, 7507 (2015).
225. Caldwell, J. D. et al. Sub-diffractional volume-confined polaritons in the natural hyperbolic material hexagonal boron nitride. *Nat. Commun.* **5**, 5221 (2014).
226. Tiwald, T. E. et al. Carrier concentration and lattice absorption in bulk and epitaxial silicon carbide determined using infrared ellipsometry. *Phys. Rev. B* **60**, 11464 (1999).
227. Aryaee Panah, M. E., Semenova, E. S. & Lavrinenko, A. V. Enhancing optical forces in InP-based waveguides. *Sci. Rep.* **7**, 3106 (2017).
228. Passler, N. C. et al. Strong coupling of epsilon-near-zero phonon polaritons in polar dielectric heterostructures. *Nano Lett.* **18**, 4285–4292 (2018).
229. Liberal, I. & Engheta, N. Manipulating thermal emission with spatially static fluctuating fields in arbitrarily shaped epsilon-near-zero bodies. *Proc. Natl. Acad. Sci. USA* **115**, 2878–2883 (2018).
230. Liberal, I., Mahmoud, A. M., Li, Y., Edwards, B. & Engheta, N. Photonic doping of epsilon-near-zero media. *Science* **355**, 1058–1062 (2017).
231. Jun, Y. C., Luk, T. S., Robert Ellis, A., Klem, J. F. & Brener, I. Doping-tunable thermal emission from plasmon polaritons in semiconductor epsilon-near-zero thin films. *Appl. Phys. Lett.* **105**, 131109 (2014).
232. Rodríguez-Fortuño, F. J., Vakil, A. & Engheta, N. Electric levitation using ϵ-near-zero metamaterials. *Phys. Rev. Lett.* **112**, 033902 (2014).
233. Jacob, Z. Hyperbolic phonon–polaritons. *Nat. Mater.* **13**, 1081–1083 (2014).
234. Dunkelberger, A. D. et al. Active tuning of surface phonon polariton resonances via carrier photoinjection. *Nat. Photonics* **12**, 50–56 (2018).
235. Ou, J. Y. et al. Ultraviolet and visible range plasmonics in the topological insulator $Bi_{1.5}Sb_{0.5}Te_{1.8}Se_{1.2}$. *Nat. Commun.* **5**, 5139 (2014).
236. Boyd, R. *Nonlinear Optics*. (Elsevier, 2008).
237. Popov, S. V. et al. Intensity-activated birefringence zero-crossing shift in $CuAlSe_2$ crystal. *Opt. Lett.* **15**, 993–995 (1990).
238. Kinsey, N. & Khurgin, J. Nonlinear epsilon-near-zero materials explained: opinion. *Opt. Mater. Express* **9**, 2793–2796 (2019).
239. Reshef, O. et al. Beyond the perturbative description of the nonlinear optical response of low-index materials. *Opt. Lett.* **42**, 3225–3228 (2017).
240. Argyropoulos, C., D'Aguanno, G. & Alù, A. Giant second-harmonic generation efficiency and ideal phase matching with a double ε-near-zero cross-slit metamaterial. *Phys. Rev. B* **89**, 235401 (2014).
241. Wen, X. et al. Doubly enhanced second harmonic generation through structural and epsilon-near-zero resonances in TiN nanostructures. *ACS Photonics* **5**, 2087–2093 (2018).
242. Hendrickson, J. R. et al. Coupling of epsilon-near-zero mode to gap plasmon mode for flat-top wideband perfect light absorption. *ACS Photonics* **5**, 776–781 (2018).
243. Hendrickson, J. R. et al. Plasmonic enhancement of epsilon-near-zero modes. in *Adv. Photonics* NpTh4C.2 https://doi.org/10.1364/NP.2018.NpTh4C.2 (OSA, 2018).
244. Kauranen, M. & Zayats, A. V. Nonlinear plasmonics. *Nat. Photonics* **6**, 737–748 (2012).
245. Scalora, M. et al. Harmonic generation from metal-oxide and metal-metal boundaries. *Phys. Rev. A* **98**, 023837 (2018).
246. De Ceglia, D., Campione, S., Vincenti, M. A., Capolino, F. & Scalora, M. Low-damping epsilon-near-zero slabs: Nonlinear and nonlocal optical properties. *Phys. Rev. B* **87**, 155140 (2013).
247. Argyropoulos, C., Chen, P.-Y., D'Aguanno, G., Engheta, N. & Alù, A. Boosting optical nonlinearities in ε-near-zero plasmonic channels. *Phys. Rev. B* **85**, 045129 (2012).
248. Argyropoulos, C., Chen, P.-Y. & Alù, A. Enhanced nonlinear effects in metamaterials and plasmonics. *Adv. Electromagn.* **1**, 46–51 (2012).
249. Yang, Y. et al. High-harmonic generation from an epsilon-near-zero material. *Nat. Phys*. (2019).
250. Vezzoli, S. et al. Optical time reversal from time-dependent epsilon-near-zero media. *Phys. Rev. Lett.* **120**, 043902 (2018).
251. Pendry, J. B. Time reversal and negative refraction. *Science* **322**, 71–73 (2008).
252. Yang, Y. et al. Femtosecond optical polarization switching using a cadmium oxide-based perfect absorber. *Nat. Photonics* **11**, 390–395 (2017).
253. Kaipurath, R. M. et al. Optically induced metal-to-dielectric transition in epsilon-near-zero metamaterials. *Sci. Rep.* **6**, 27700 (2016).
254. Shaltout, A., Kildishev, A. & Shalaev, V. Time-varying metasurfaces and Lorentz non-reciprocity. *Opt. Mater. Express* **5**, 2459–2467 (2015).
255. Ferdinandus, M. R., Gengler, J., Kinsey, N. & Urbas, A. Epsilon near-zero nonlinear optical measurements of titanium nitride thin films. in *Conf. Lasers Electro-Optics* JTu2A.130 https://doi.org/10.1364/CLEO_AT.2018.JTu2A.130 (OSA, 2018).
256. Low, T. et al. Plasmons and screening in monolayer and multilayer black phosphorus. *Phys. Rev. Lett.* **113**, 106802 (2014).
257. Shcherbakov, M. R. et al. Nonlinear manifestations of photon acceleration in rapidly evolving semiconductor metasurfaces. in *Conf. Lasers Electro-Optics* FTh1D.2 https://doi.org/10.1364/CLEO_QELS.2018.FTh1D.2 (OSA, 2018).
258. Khurgin, J. B. & Kinsey, N. *Adiabatic frequency conversion: it is all about group velocity. arXiv* **1906**, 04849 (2019).
259. Ciracì, C., Pendry, J. B. & Smith, D. R. Hydrodynamic model for plasmonics: a macroscopic approach to a microscopic problem. *ChemPhysChem* **14**, 1109–1116 (2013).
260. Ginzburg, P., Krasavin, A. V., Wurtz, G. A. & Zayats, A. V. Nonperturbative hydrodynamic model for multiple harmonics generation in metallic nanostructures. *ACS Photonics* **2**, 8–13 (2015).
261. Westerberg, N., Cacciatori, S., Belgiorno, F., Piazza, F. D. & Faccio, D. Experimental quantum cosmology in time-dependent optical media. *New J. Phys.* **16**, 075003 (2014).
262. Faccio, D. Laser pulse analogues for gravity and analogue Hawking radiation. *Contemp. Phys.* **53**, 97–112 (2012).
263. Butera, S., Westerberg, N., Faccio, D. & Öhberg, P. Curved spacetime from interacting gauge theories. *Class. Quantum Gravity* **36**, 034002 (2019).
264. Fleury, R. & Alù, A. Enhanced superradiance in epsilon-near-zero plasmonic channels. *Phys. Rev. B* **87**, 201101 (2013).
265. Minkov, M., Williamson, I. A. D., Xiao, M. & Fan, S. *Zero-index bound states in the continuum. Phys. Rev. Lett.* **121**, 263901 (2018).
266. Limonov, M. F., Rybin, M. V., Poddubny, A. N. & Kivshar, Y. S. Fano resonances in photonics. *Nat. Photonics* **11**, 543–554 (2017).
267. Hsu, C. W., Zhen, B., Stone, A. D., Joannopoulos, J. D. & Soljačić, M. Bound states in the continuum. *Nat. Rev. Mater.* **1**, 16048 (2016).

268. Monticone, F., Doeleman, H. M., Den Hollander, W., Koenderink, A. F. & Alù, A. Trapping light in plain sight: embedded photonic eigenstates in zero-index metamaterials. *Laser Photon. Rev.* **12**, 1700220 (2018).
269. Cai, W. & Shalaev, V. M. *Optical Metamaterials: Fundamentals and Applications*. (Springer, 2009).
270. Poddubny, A., Iorsh, I., Belov, P. & Kivshar, Y. Hyperbolic metamaterials. *Nat. Photonics* **7**, 948–957 (2013).
271. Gao, J. et al. Experimental realization of epsilon-near-zero metamaterial slabs with metal-dielectric multilayers. *Appl. Phys. Lett.* **103**, 051111 (2013).
272. Vassant, S., Hugonin, J.-P., Marquier, F. & Greffet, J.-J. Berreman mode and epsilon near zero mode. *Opt. Express* **20**, 23971–23977 (2012).
273. Taliercio, T., Guilengui, V. N., Cerutti, L., Tournié, E. & Greffet, J.-J. Brewster "mode" in highly doped semiconductor layers: an all-optical technique to monitor doping concentration. *Opt. Express* **22**, 24294–24303 (2014).
274. Vassant, S. et al. Epsilon-near-zero mode for active optoelectronic devices. *Phys. Rev. Lett.* **109**, 237401 (2012).
275. Baranov, D. G., Krasnok, A., Shegai, T., Alù, A. & Chong, Y. Coherent perfect absorbers: linear control of light with light. *Nat. Rev. Mater.* **2**, 17064 (2017).
276. Minn, K., Anopchenko, A., Yang, J. & Lee, H. W. H. Excitation of epsilon-near-zero resonance in ultra-thin indium tin oxide shell embedded nanostructured optical fiber. *Sci. Rep.* **8**, 2342 (2018).
277. Shrestha, S. et al. Indium tin oxide broadband metasurface absorber. *ACS Photonics* **5**, 3526–3533 (2018).
278. Jahani, S. & Jacob, Z. All-dielectric metamaterials. *Nat. Nanotechnol.* **11**, 23–36 (2016).
279. Schuller, J. A., Zia, R., Taubner, T. & Brongersma, M. L. Dielectric metamaterials based on electric and magnetic resonances of silicon carbide particles. *Phys. Rev. Lett.* **99**, 107401 (2007).
280. Filonov, D. S. et al. Experimental verification of the concept of all-dielectric nanoantennas. *Appl. Phys. Lett.* **100**, 201113 (2012).
281. Staude, I. et al. Tailoring directional scattering through magnetic and electric resonances in subwavelength silicon nanodisks. *ACS Nano* **7**, 7824–7832 (2013).
282. Pendry, J. B., Holden, A. J., Robbins, D. J. & Stewart, W. J. Magnetism from conductors and enhanced nonlinear phenomena. *IEEE Trans. Microw. Theory Tech.* **47**, 2075–2084 (1999).
283. Cai, W. et al. Metamagnetics with rainbow colors. *Opt. Express* **15**, 3333–3341 (2007).
284. Wang, H. et al. Extended Drude model for intraband-transition-induced optical nonlinearity. *Phys. Rev. Appl.* **11**, 064062 (2019).
285. Conforti, M. & Della Valle, G. Derivation of third-order nonlinear susceptibility of thin metal films as a delayed optical response. *Phys. Rev. B* **85**, 245423 (2012).
286. Del Fatti, N. et al. Nonequilibrium electron dynamics in noble metals. *Phys. Rev. B* **61**, 16956 (2000).
287. Shin, T., Teitelbaum, S. W., Wolfson, J., Kandyla, M. & Nelson, K. A. Extended two-temperature model for ultrafast thermal response of band gap materials upon impulsive optical excitation. *J. Chem. Phys.* **143**, 194705 (2015).
288. Zavelani-Rossi, M. et al. Transient optical response of a single gold nanoantenna: the role of plasmon detuning. *ACS Photonics* **2**, 521–529 (2015).
289. Sze, S. M. & Ng, K. K. *Physics of Semiconductor Devices 3rd edn*. (Wiley, 2006).
290. Strauss, U., Rühle, W. W. & Köhler, K. Auger recombination in intrinsic GaAs. *Appl. Phys. Lett.* **62**, 55–57 (1993).
291. Shcherbakov, M. R. et al. Ultrafast all-optical tuning of direct-gap semiconductor metasurfaces. *Nat. Commun.* **8**, 17 (2017).
292. Bennett, B. R., Soref, R. A. & Del Alamo, J. A. Carrier-induced change in refractive index of InP, GaAs and InGaAsP. *IEEE J. Quantum Electron.* **26**, 113–122 (1990).
293. Benjamin, S. D., Loka, H. S., Othonos, A. & Smith, P. W. E. Ultrafast dynamics of nonlinear absorption in low-temperature-grown GaAs. *Appl. Phys. Lett.* **68**, 2544–2546 (1996).
294. Gupta, S. et al. Subpicosecond carrier lifetime in GaAs grown by molecular beam epitaxy at low temperatures. *Appl. Phys. Lett.* **59**, 3276–3278 (1991).
295. Ortiz, V., Nagle, J., Lampin, J.-F., Péronne, E. & Alexandrou, A. Low-temperature-grown GaAs: Modeling of transient reflectivity experiments. *J. Appl. Phys.* **102**, 043515 (2007).
296. Zhao, H., Wang, Y., Capretti, A., Negro, L. D. & Klamkin, J. Broadband electroabsorption modulators design based on epsilon-near-zero indium tin oxide. *IEEE J. Sel. Top. Quantum Electron.* **21**, 192–198 (2015).
297. Ginn, J. C., Jarecki, R. L., Shaner, E. A. & Davids, P. S. Infrared plasmons on heavily-doped silicon. *J. Appl. Phys.* **110**, 043110 (2011).
298. Kehr, S. C. et al. Near-field examination of perovskite-based superlenses and superlens-enhanced probe-object coupling. *Nat. Commun.* **2**, 249 (2011).
299. Kyoung, J. et al. Epsilon-near-zero meta-lens for high resolution wide-field imaging. *Opt. Express* **22**, 31875–31883 (2014).
300. Streyer, W. et al. Engineering absorption and blackbody radiation in the far-infrared with surface phonon polaritons on gallium phosphide. *Appl. Phys. Lett.* **104**, 131105 (2014).

Acknowledgements
N.K. would like to acknowledge support from the Air Force Office of Scientific Research Young Investigator Program (FA9550-18-1-0151), the Virginia Microelectronics Consortium Seed Grant and the Virginia Commonwealth University Presidential Research Quest Fund. The Purdue team acknowledges support from the U.S. Department of Energy, Office of Basic Energy Sciences, Division of Materials Sciences and Engineering under award DE-SC0017717 (A.B. and V.M.S.) and the Air Force Office of Scientific Research under award FA9550-18-1-0002 (C.D.).

Author contributions
N.K. and C.D. compiled and prepared the manuscript. All authors contributed to the editing and revision of the manuscript.

Competing interests
The authors declare no competing interests.

Publisher's note